ABSTRACT

Oncomodulin Alters the Ca^{2+}-Regulating Network in Cochlear Outer Hair Cells

Forrest Jones

Director: Dwayne Simmons, Ph.D.

The study of hair cells (HCs) located in the cochlea of the inner ear is beginning to unveil the mysteries of hearing loss. HCs transform sound waves into electrical signals that are sent to the brain for interpretation and are essential for hearing. In previous work, analysis of the expression of cytosolic calcium (Ca^{2+})-binding proteins (CaBPs) in HCs has illuminated potential mechanisms for the development, maintenance, and deterioration of hearing. In mice where a particular CaBP, Oncomodulin (OCM), was genetically engineered to be missing, hearing loss was accelerated. In fact, 4 months after birth, they were essentially deaf. Thus, OCM is a CaBP of interest because it is directly involved in the maintenance of hearing. To determine how OCM maintains hearing, this thesis project examined the impact that OCM had on Ca^{2+} regulator proteins within the outer hair cell (OHC). Data was collected using reverse transcription quantitative polymerase chain reaction (RT-qPCR) for quantitative analysis and immunohistochemistry for qualitative analysis. In OHCs, the engineered absence of OCM altered the expression of 3 purinergic receptors, 2 voltage-gated Ca^{2+} channels, an intracellular Ca^{2+} buffer, and an ATP-driven Ca^{2+} exporter, which suggests that OCM modulates the OHC Ca^{2+}-regulating network in order to establish intracellular Ca^{2+} balance.

APPROVED BY DIRECTOR OF HONORS THESIS:

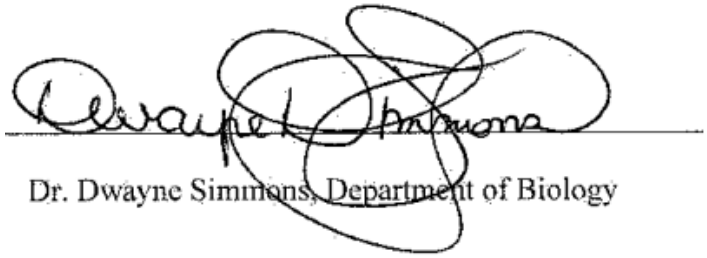

Dr. Dwayne Simmons, Department of Biology

APPROVED BY THE HONORS PROGRAM:

_____

Dr. Andrew Wisely, Interim Director

DATE: _____

ONCOMODULIN ALTERS THE Ca^{2+}-REGULATING NETWORK IN COCHLEAR OUTER HAIR CELLS

A Thesis Submitted to the Faculty of

Baylor University

In Partial Fulfillment of the Requirements for the

Honors Program

By

Forrest Jones

Waco, Texas

May 2021

TABLE OF CONTENTS

LIST OF FIGURES

LIST OF TABLES

ACKNOWLEDGEMENTS

I would like to thank Dr. Dwayne Simmons for the opportunity to conduct this project, the members of the Simmons Lab for their encouragement and guidance, and my parents for their endless support. I also want to thank the Folmar Research Fund and the Baylor University Honors College for their financial support through this project. Lastly, I want to thank God for his guidance and blessings throughout my undergraduate career.

CHAPTER ONE

Introduction

1.1 Statement of Purpose

Ca^{2+} and Ca^{2+}-regulators in OHCs play an intricate role in the process of hearing. Experiments by Hackney et al. (2005), Pangrsic et al. (2015), and Tong et al. (2016) suggest that OCM, a Ca^{2+} buffer protein in OHCs, is directly involved with the maintenance of hearing. However, the exact mechanism by which OCM maintains hearing remains unknown.

The purpose of this thesis project is to illuminate how OCM might operate within the OHC Ca^{2+}-regulating network. Understanding OCM's role in OHC Ca^{2+} regulation will yield insight into how it maintains hearing. The role of OCM in OHC Ca^{2+} regulation was examined by analyzing differences in Ca^{2+} regulator gene/protein expression between *Ocm* wild-type (WT) and *Ocm* knock out (KO) mice. Changes in Ca^{2+} regulator gene/protein expression in the absence of OCM highlight potential mechanisms through which OCM maintains hearing. The results shows that the absence of OCM changes gene/protein expression in OHC Ca^{2+} regulators from postnatal day 0 (P0) to postnatal day 6 (P6). Altering Ca^{2+} regulator expression may compensate for the loss of OCM for a while, but the compensation is not sustainable. This is evidenced by the progressive, early-onset deafness that occurs in *Ocm* KO mice. Thus, OCM may maintain hearing by

regulating members of the OHC Ca^{2+}-regulating network in order to sustain intracellular Ca^{2+} balance.

This paper is divided into four chapters. The first chapter reviews sensorineural hearing loss, cochlear anatomy, and HC physiology to show how OHC Ca^{2+} and Ca^{2+} regulators are involved with hearing. This chapter also introduces members of the OHC Ca^{2+} regulatory network[1]: calcium importers (*Cacna1c, Cacna1d*, *P2rx2/*P2X2, *P2rx3/*P2X3, and *P2rx7/*P2X7), calcium exporters (*Atp2b2*), and two calcium buffers (*Pvalb/*aPV and *Ocm*/OCM). The functions and locations of these Ca^{2+} regulators in OHCs are discussed in detail in section 1.5. An understanding of their function and location enables speculation of how and why OCM interacts with the OHC Ca^{2+}-regulating network. The second chapter describes the quantitative and qualitative methods used to measure the impact of OCM on the OHC Ca^{2+}-regulating network. The third chapter displays the results. Finally, the fourth chapter discusses results, applications, and future directions of study.

[1] Gene names are in italics. Protein names are in regular font. Gene expression was examined for all Ca^{2+} regulators while protein expression was examined for a select few.

1.2 Sensorineural Hearing Loss

Presbycusis broadly refers to the gradual hearing loss that occurs with age. It is a multifaceted disease that debilitates nearly 466 million people worldwide (WHO). As a progressive disease, presbycusis is often most severe during old age. Today, approximately 35% of adults over age 65 and 50% over age 75 suffer from hearing loss, but hearing disabilities are not limited to adults. The World Health Organization (WHO) estimates that 34 million of those disabled by hearing loss are children, demonstrating that age is not the sole determinant of hearing loss. Factors contributing to this phenomenon are abnormalities in the outer and middle ear (tympanic membrane, malleus, incus, and stapes) morphology and general sensorineural hearing loss. This project focuses on the latter. Sensorineural hearing loss is a broad term referring to the progressive decline of hearing due to damage of the HCs and/or spiral ganglia within the cochlea. Damage to HCs is primarily caused by three factors: exposure to ototoxic substances (e.g., aminoglycoside antibiotics and salicylates that are toxic to sensory HCs and neurons), prolonged exposure to high-intensity noise, and congenital disorders. The deleterious effects imposed by these factors on HCs escalate with age, causing a gradual decline in hearing ability. Studies have shown that in deaf animals, HCs disappear or change morphology (Dallos, 1996). Once dead, HCs cannot regenerate, thereby making hearing loss irreversible (Dallos, 1996). There is ongoing research that seeks to address this problem by using transcription factors unique to HCs to differentiate supporting cells into new HCs (Yamoah et al., 2020), but that is beyond the scope of this project.

HCs express an array of cytosolic and transmembrane proteins that contribute to their dynamic and finely tuned process of mechanotransduction— the process of converting sound waves into electrical signals that are sent to our primary auditory cortex (via the ascending auditory pathway) for processing. In order to understand mechanotransduction and how it involves Ca^{2+}, cochlear anatomy and HC physiology must first be discussed.

1.3 Cochlear Anatomy

Embedded in the temporal bone, the cochlea lies medial to the middle ear (ossicles and tympanic cavity), inferior to the vestibule and semicircular canals, and superior to the Eustachian tube. Its snail-shell-shaped body is encased in a bony labyrinth. Deep to the bony labyrinth lies the membranous labyrinth which lines the cavity of the inner ear.

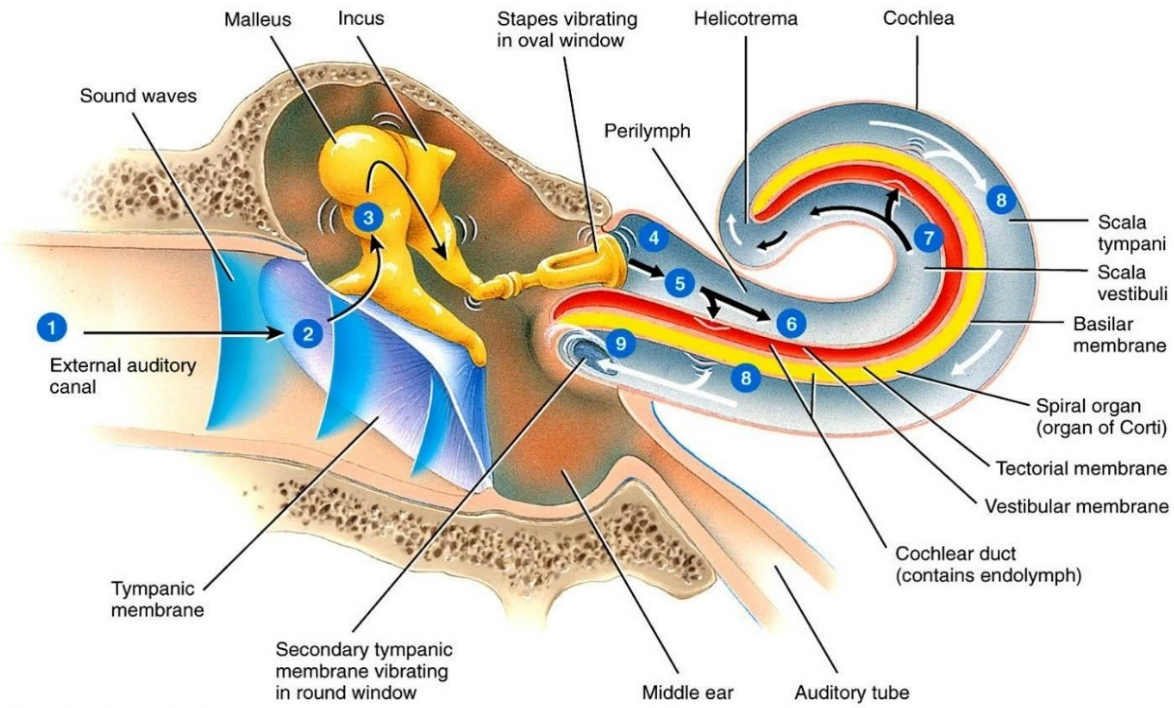

Figure 1**.** The passage of sound stimuli to and through the cochlea (*Principles of Human Anatomy, 12th ed.*, Tortora and Nielsen).

Within the turns of the cochlea are three fluid-filled, tubular canals that run parallel to each other from the base to the helicotrema (or apex; Fig. 1). The three canals are composed of fluids that create an electrochemical gradient in the cochlea. First, the scala vestibuli is responsible for transmitting sound waves created by the mechanical banging of the stapes [end plate] on the oval window to the HCs. This canal is composed of **perilymph** (-70mV), a fluid high in sodium (138 mM) and low in potassium (6.9 mM; Bosher and Warren, 1968; Fig. 2). It also has a Ca^{2+} concentration of 1.3 mM that sustains proteins on the OHC membrane that (Fettiplace et al., 2018). Second, the scala tympani transmits the sound waves reflected from the helicotrema to the round window

near the base of the cochlea. It, too, is filled with perilymph. The scala vestibuli and scala tympani are joined at the helicotrema, enabling a unidirectional flow of fluid pressure waves from the scala vestibuli to the scala tympani that stimulate the scala media, which lies between the scala vestibuli and tympani. The scala media is physically and chemically separated from the scala vestibuli by Reissner's membrane and from the scala tympani (see Fig. 2) by the supporting cells (discussed later) via tight junctions (Dallos, 1996). Within this tubular compartment lies **endolymph** (+80mV), a fluid characterized by a high concentration of potassium (154 mM) and a low concentration of sodium (91 mM; Bosher and Warren, 1968)—opposite of perilymph in the adjacent scala vestibuli and scala tympani. It also has a Ca^{2+} concentration of 1 μM (Fettiplace et al., 2018). Endolymph is maintained by the stria vascularis, which is a 3-cell layer of vascular epithelia along the lateral wall of the scala media that nourishes the organ of Corti (a structure within the cochlea housing HCs and supporting cells) and creates endolymph (Pickles, 1988). The chemical composition of endolymph and perilymph create an electrochemical gradient across the organ of Corti that enables HCs to function. How the electrochemical gradient is maintained is discussed in the section on the organ of Corti and supporting cells (section 1.3b), and how the electrochemical gradient enables HCs to function is discussed in the section on HC physiology (section 1.4).

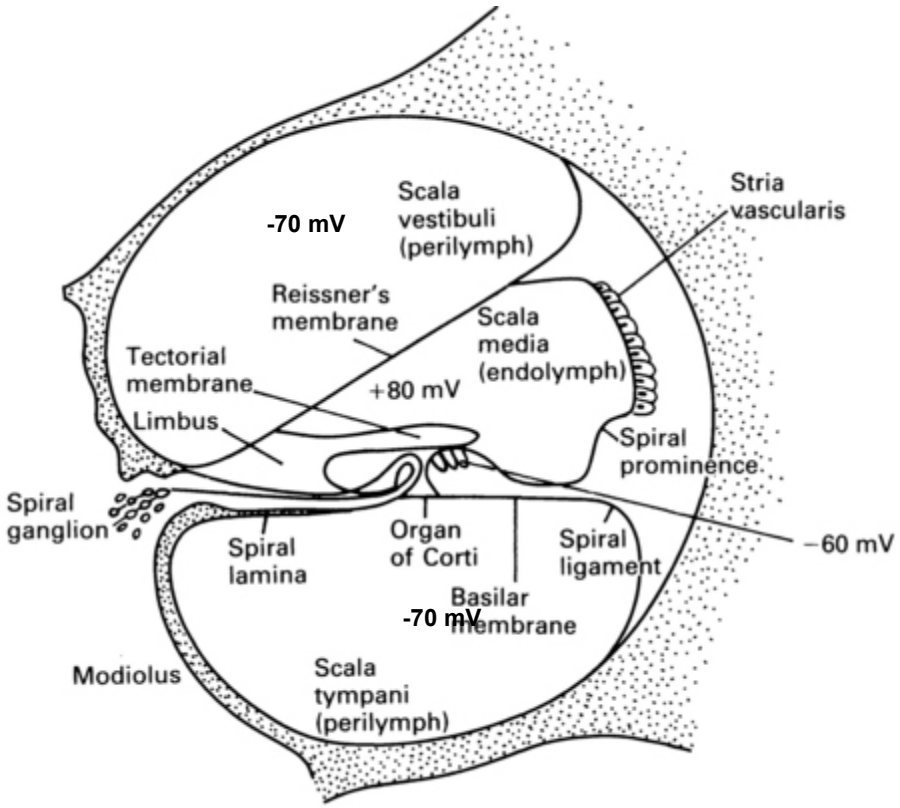

Figure 2: Cross section of the cochlea (Pickles J O, 1985).

1.3a Basilar Membrane

The cochlear basilar membrane is structured in a way that enables the detection of different frequencies in a sound wave. It thickens along its length from the base of the cochlea to the apex (Pickles, 1988). The thickness gradient of the basilar membrane makes the cochlea *tonotopic*, or spatially arranged to register different frequencies. A sound-induced travelling wave is maximally amplified at specific regions along the length of the cochlea, with high frequency sounds producing maximum stimulation in basal regions and low frequency sounds producing maximum stimulation toward the apex

(Pickles, 1988). This is because high frequency sounds resonate better in the thick basal portion of the basilar membrane, while low frequency sounds resonate better in the thin apical portion of the basilar membrane (Dallos, 1996). In humans, the boundaries of sound frequency detection lie at 20 to 20,000 Hz. In mice, which this study utilized, sound frequencies are normally detected from 1 to 80 kHz. The topic of tonotopicity will return in the discussion of sound discrimination by OHCs (Table 1.2).

1.3b The Organ of Corti and Supporting Cells

The Organ of Corti, discovered by Alfonso Giacomo Gaspare Corti in 1851 (Betlejewski, 2008), rests on the basilar membrane. Running from the base to the apex of the cochlea, the Organ of Corti consists of a sheet of epithelium composed of HCs and supporting cells (2 rows of pillar cells, 3 rows of Deiter cells (DCs), Hensen's cells, border cells, and inner phalangeal cells (Dallos, 1996). The HCs are situated above DCs and inner phalangeal cells and sit adjacent to Pillar cells (Fig. 3). In addition to rendering HCs physical support, DCs, inner phalangeal cells, and pillar cells play a critical role in the ion mechanics of the organ of Corti by forming the reticular lamina. The reticular lamina consists of HC apical membranes, phalangeal actin processes from DCs and inner phalangeal cells, and tight junctions (Dallos, 1996). It imposes a barrier impermeable to the ions of the endolymph located in the scala media. Thus, the supporting cells of the organ of Corti are responsible for maintaining the electrochemical gradient needed for mechanotransduction (table

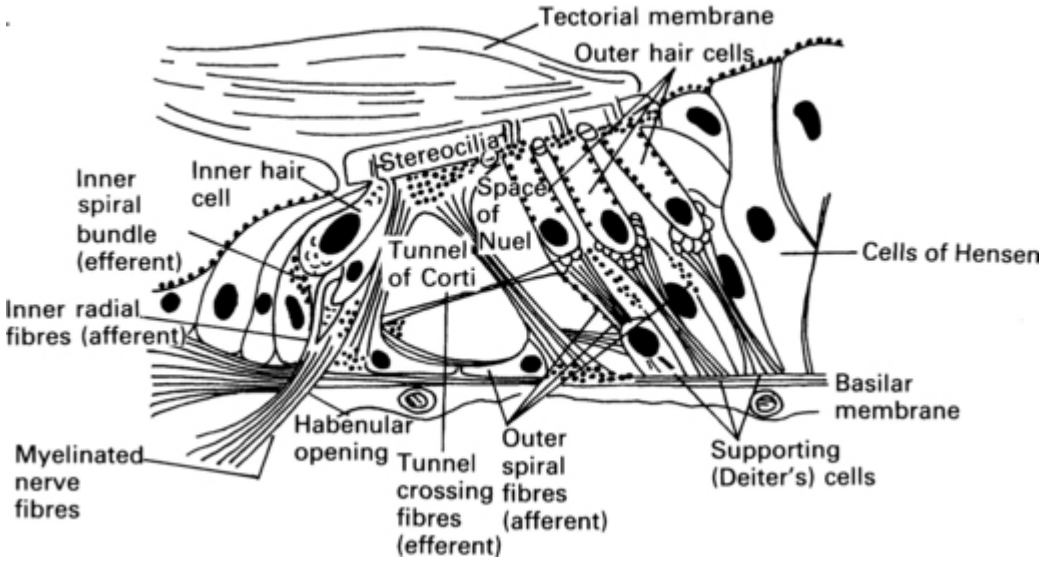

Figure 3**:** Diagram of the Organ of Corti (Durrant J D & Lovrinic J H 1984)

The other major component of the organ of Corti is the tectorial membrane, a gel-like, viscoelastic layer of collagen (50%), glycoproteins (25%), and proteoglycans (25%; Thalmann et al, 1986; Ghaffari et al, 2007). It is anchored to the spiral limbus on the medial wall of the scala media and is thought to be connected with the stereocilia (Dallos, 1996). Stereocilia are rigid cilia with an actin core and mechanically-activated ion channels. They protrude from the apical membrane of HCs and reticular lamina into the endolymph. Another model suggests that while the tectorial membrane is not physically attached to stereocilia, its oscillating movement during noise stimulation enables it to brush the stereocilia to activate a cellular response. In either model, the tectorial membrane displaces HC stereocilia as the basilar membrane oscillates at maximum amplitude at resonant frequency, which is specified by the specific thickness of the

basilar membrane (Pickles, 1988). Displacing HC stereocilia elicits an excitatory response within the HC that begins the mechanotransduction pathway, which will be discussed with HC physiology.

1.4 HC Anatomy and Physiology

There are two types of HCs in the cochlea: inner and outer HCs (IHCs and OHCs). They differ in shape, composition, and function. IHCs serve as the organ of Corti's primary sensory epithelia and are arranged in 1 row from the base to the apex of the cochlear spiral. They are flask-shaped in appearance, have a central nucleus, scattered organelles, and 3 to 4 rows of stereocilia in a straight line, growing in length laterally (Fig. 4). In the basal region of the IHC lie synaptic ribbons, clusters of proteins along the basal cell membrane that expedite the process of neurotransmitter vesicle exocytosis (Pickles, 1988; Khimich et al., 2005). Upon Ca^{2+} influx, vesicles of glutamate form at the base of IHCs with the help of non-neuronal SNARE proteins (Nouvian et al., 2011). The vesicles of glutamate are released from the presynaptic membrane with the help of synaptic ribbons. As a result, synaptic ribbons make IHCs effective transmitters of afferent information.

Collectively known as the "cochlear amplifier," OHCs increase IHC stimulation from sound stimuli. The mechanism for this process is shown in Table 1. OHCs run parallel to IHCs and are arranged in 3 rows from the base to the apex of the cochlear spiral (Fig. 4). They have a cylindrical shape, a basal nucleus, 3 to 4 rows of stereocilia, and organelles cluster below the cuticular plate as well as below the nucleus. This is

largely due to the great levels of activity occurring in these regions of the cell (Dallos, 1996). While the OHC has presynaptic ribbons, there are much fewer than in IHCs. This aligns with the fact that OHCs have minimal direct contribution to afferent signaling. Despite having sparse afferent neuron synapses, OHCs are immensely important to hearing because they enable pressure waves to be mechanotransduced into electrical signals sent by IHCs (Table 1).

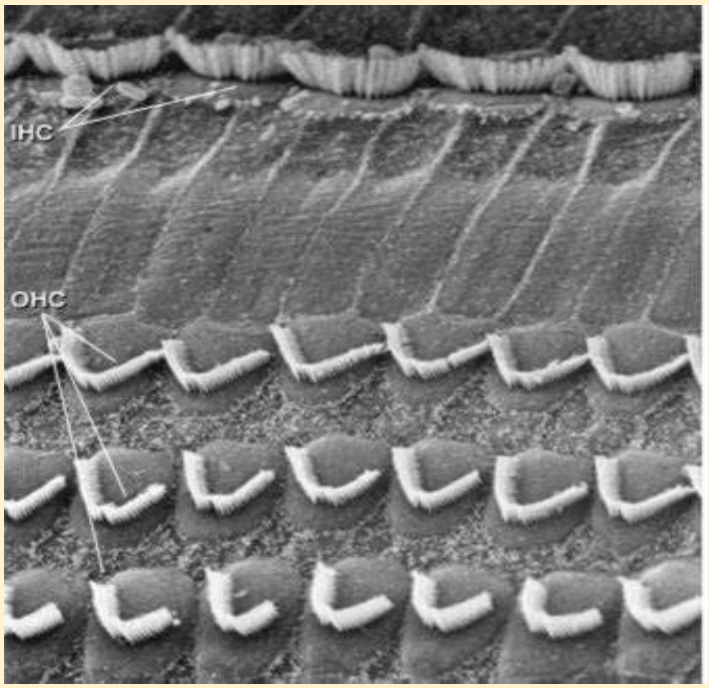

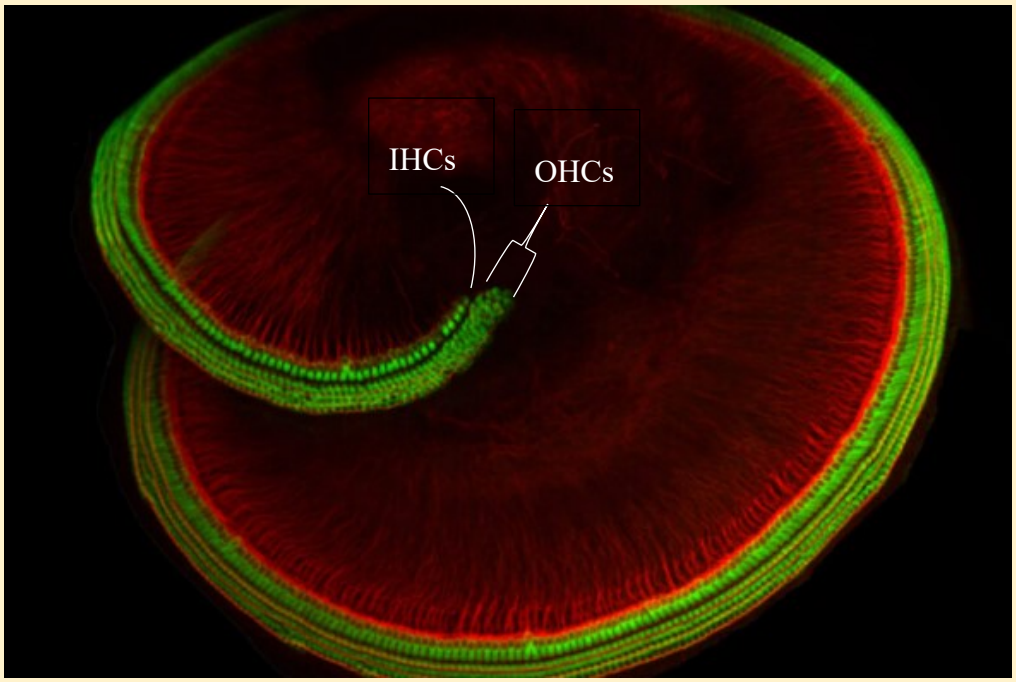

Figure 4. A) TEM demonstrating the organization of cochlear HCs. Image was taken from VR4Hearig Loss. B) Immunohistochemistry image demonstrating HC location along the spiral. Image taken from Harvard Medical School Holt lab. The spiral is found within the bony labyrinth of the cochlea.

Stereocilia play a crucial role in the mechanotransduction process. When HC stereocilia are moved during basilar membrane vibration, the stereocilia unit moves in the same direction, creating tension in the cadherin-23/protocadherin-15 “tip links” that rest on the tips of stereocilia and attach to mechanoelectrical transduction channels (METs) located on the surface of each stereocilium (Fig. 5; Dallos et al., 1996). Tip links unify stereocilia bundle movement (Fig. 6). Further, as cadherins, tip link protein function is dependent upon Ca^{2+}, which is present in small quantities in the endolymph. Tension between tip links pulls open the MET (1-4 per stereocilium) gate to the endolymph, allowing K^{+} influx down each stereocilium to trigger a opening of VGCCs resulting in membrane depolarization (Pickles et al., 1984; Pickles, 1996; Corns et al. 2018). IHCs (-45mV) are less sensitive to depolarization than OHCs (-60mV) (Pickles, 1988). In other words, a larger voltage change is required for IHC activation than OHC activation. The intensity of the sound wave affects the duration of basilar membrane vibration and the extent to which the stereocilia bend underneath the tectorial membrane. Both the duration and extent of stereocilia excitation determines the tensile force applied to the chain links and thus the size of the K^{+} potential entering the HC. Thus, the greater the stimulation, the greater the Ca^{2+} depolarization response.

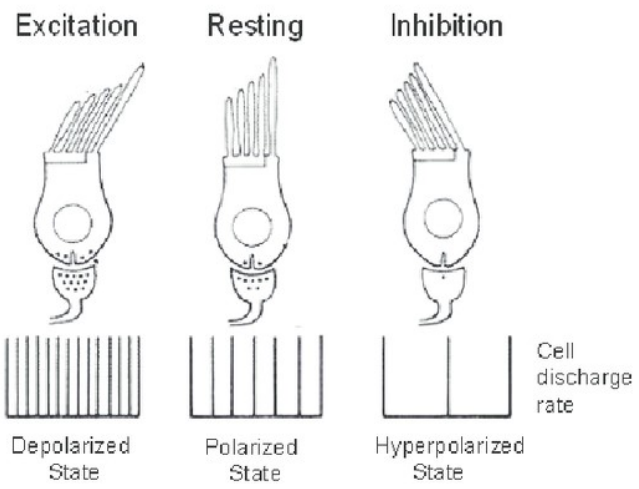

Figure 5: IHCs during an excitation cycle. Image taken from *Auditory function: Physiology and function of the hearing system* (Emanuel et al. 2009).

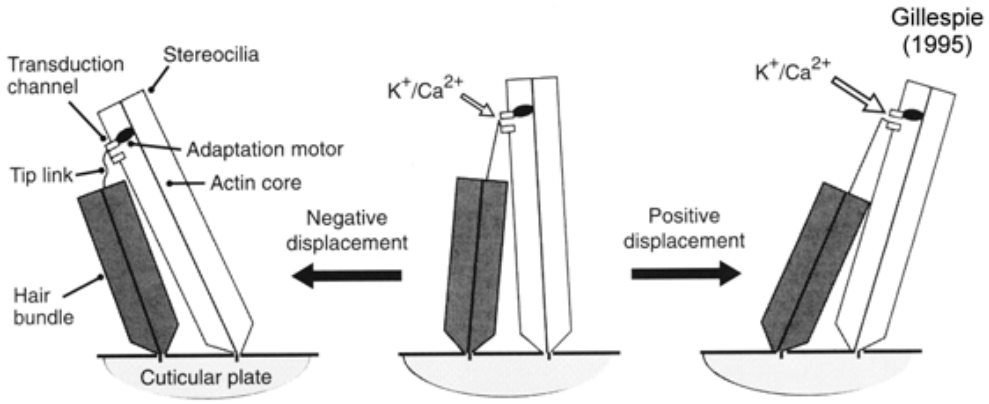

Figure 6**.** Activation of the stereocilia bundle during stimulation. When moved by the tectorial membrane, HC stereocilia move in unison to one side, tightening tip links, opening MET channels to endolymph, and allowing K^+ influx into the HC from the stereocilia. The maximum MET current varies tonotopically, the amplitude increasing from 1.7 nA at the apical turn to as much 7 nA at the basal turn (Johnson et al., 2011). Ca^{2+} is a cofactor in this process (Pickles, 1988).

OHCs possess some capacity for sensory transmission, but they primarily specialize in sound modulation and amplification. The ways in which this is accomplished are outlined below. Table 1 outlines the way in which OHCs can protect our HCs from damaging noise (modulation), and Table 2 outlines the way in which OHCs can amplify sounds to improve frequency discrimination.

Table 1. OHC sound discrimination/amplification relies on cell depolarization.

1. Attempt to focus on a particular sound.
2. Presynaptic efferent cholinergic fibers innervating the OHC release acetylcholine (ACh) into the synapse.
3. ACh binds to postsynaptic nicotinic acetylcholine receptors on the basal surface of the OHC.
4. Ach binding causes extracellular Ca^{2+} influx and subsequent Ca^{2+} induced Ca^{2+} release (CICR) from intracellular cisternae (SERCA). The result is a large-scale release of intracellular Ca^{2+} and depolarization.
5. The contractile protein, prestin, located in the lateral wall of the OHC, **contracts during depolarization**.
6. The OHC shortens, causing an **upward bowing of the basilar membrane, improving its range of motion.** Squeezing the HCs and tectorial membrane closer together causes endolymph to **displace the hair bundle away from the tallest stereocilia.**
7. Greater HC activation ensues.
8. Improved ability to discern low-intensity noise as well as parse frequencies from one another and background noise.

Table 2. OHC sound modulation/protection relies on hyperpolarization of the cell.

1. High intensity sound waves in ear cause the brain to send efferent messages to the cochlea to prevent damage.
2. Presynaptic efferent cholinergic fibers innervating the OHC release acetylcholine (ACh) into the synapse.
3. ACh binds to postsynaptic nicotinic acetylcholine receptors on the basal surface of the OHC.
4. Ach binding causes extracellular Ca^{2+} influx and subsequent Ca^{2+} induced Ca^{2+} release (CICR) from intracellular cisternae (SERCA). The result is a large-scale release of intracellular Ca^{2+} and depolarization.
5. Intracellular Ca^{2+} is bound by the Ca^{2+}sensor, calmodulin, in the cytosol. The Ca^{2+}-calmodulin complex binds to a transmembrane small-conductance K^+ channel (SK2), stimulating the channel to open.
6. This causes K^+ to efflux, hyperpolarizing the OHC.
7. The contractile protein, prestin, located in the lateral wall of the OHC, **relaxes during hyperpolarization**
8. The OHC lengthens, causing a **downward bowing of the basilar membrane, restricting its full range of motion** and allowing endolymph to rush into the space between HCs and the tectorial membrane, thereby **displacing the hair bundle away from the tallest stereocilia.**
9. HC stimulation from high-intensity noise is reduced by reduced basilar membrane resonance. As a result, less damage is inflicted on IHCs and OHCs, and IHCs deliver less intense signals to the brain. Hearing sensitivity becomes temporarily dampened.

Hearing without OHCs has been compared to listening to somebody speak from the pool side while sitting 6 feet underwater.

1.5 Ca^{2+} and Ca^{2+} Regulators in the HC

With cochlear anatomy, HC anatomy, and general OHC physiology reviewed, the role of Ca^{2+} in the mechanotransduction process will be discussed. Specifically, the role of certain OHC proteins in intracellular Ca^{2+} regulation will be reviewed.

To preface, OHCs are of particular interest when studying the role of Ca^{2+} regulators in hearing loss for four reasons. First, they are directly involved with the modulation and protection of hearing (Patuzzi et al., 1989; Hallworth, 1997). Second, OHCs are sentinels of hearing loss. They are more susceptible to damage by excessive noise exposure, ototoxins, and age than IHCs (Furness, 2015). OHCs in the basal cochlea are particularly vulnerable to damage. It is believed that relatively small OHC size (lower capacitance) and lower volume of Ca^{2+} exporters reduce their ability to handle intracellular Ca^{2+} (Fettiplace and Nam, 2018). The inability of basal OHCs to effectively handle Ca^{2+} renders them susceptible to damage (Fettiplace and Nam, 2018), which shows that Ca^{2+} regulation is essential to OHC survival. Third, IHCs have about one tenth the concentration of proteinaceous Ca^{2+} buffers as OHCs (Chen et al., 2012). The large amount of proteinaceous Ca^{2+} buffer in OHCs, similar only to the millimolar concentrations of alpha-parvalbumin in skeletal muscle, implies that Ca^{2+} has an important signaling role in OHCs (Fettiplace and Nam, 2018). Finally, only about one

percent of the Ca^{2+} that enters a cell remains free, which suggests the presence of a robust Ca^{2+}-regulating network in the HCs (Fettiplace and Nam, 2018). The intracellular Ca^{2+} concentration is approximately 100–200 nM (Szücs et al., 2004; Di Leva et al, 2008).

K^+ and Ca^{2+} are the primary ions involved with the OHC mechanotransduction and depolarization/repolarization cycle. As endolymphatic K^+ enters OHCs via MET channels, the OHC endures a graded potential that stimulates voltage-gated Ca^{2+} channels (VGCCs) along the basolateral membranes of the HC to open, which in turn stimulates CICR from SERCA channels in the ER-like subsurface cisternae (Corns et al. 2018). Regulation of Ca^{2+} influx in OHCs equates to regulation of the mechanotransduction process. Six proteins involved with OHC Ca^{2+} regulation are reviewed below.

VGCCs have several isoforms, but of interest in this project are the voltage-gated L-type Ca^{2+} channels, **Ca_v1.2** and **Ca_v1.3**. Ca_v1.2 and Ca_v1.3 differ in their distribution around the body and in their transmembrane pore-forming α-1 subunits: α-1c (Ca_v1.2) and α-1d (Ca_v1.3; Hu et al., 2017; Fig. 7A-B). The α1-subunit, which contains approximately 2000 amino acid residues, is organized into four repeated domains (I to IV), each of which contains six transmembrane segments (S1 to S6) with a pore between S5 and S6 (Fig. 7A). The alternating positively charged arginine or lysine residues at every third or fourth position in S4 of each domain regulate voltage sensitivity (Ca_v1.2 is less sensitive to depolarization than Ca_v1.3; North et al., 2002). Four negatively charged glutamate residues on the pore loop located between S5 and S6 are responsible for the Ca^{2+} selectivity of the channels. The other subunits are responsible for trafficking, anchorage,

and regulatory functions (Kushnir and Marx, 2018; Lipscombe et al., 2004). In OHCs, $Ca_v1.2$ and $Ca_v1.3$ were detected by RNA seq during neonatal development by Scheffer et al (2015). Further, a mutation in the α-1d pore subunit of $Ca_v1.3$ has been implicated in deafness in mice and in humans as sinoatrial node dysfunction and deafness syndrome (SANDD syndrome; Vazquez et al. 2004; Baig et al, 2010). $Ca_v1.2$ mutations have not yet been shown to cause sensorineural deafness.

$Ca_v1.2$ and $Ca_v1.3$ share similar functions. After noise-induced activation of OHCs elicits an MET current from the stereocilia, the diffusion potential travels into the body of the OHC. The newly polarized cell membrane then unlocks the voltage-gate of $Ca_v1.2$ and $Ca_v1.3$, which in turn causes CICR. The result is a large influx of Ca^{2+} into the OHC cytoplasm after noise stimulation, leading to OHC depolarization and subsequent sound amplification (Table 2).

Interestingly, $Ca_v1.2$ and $Ca_v1.3$ contribute differently to the genesis of the Ca^{2+} depolarization in OHCs (-60mV; Fig 7C). $Ca_v1.2$ is a classic L-type VGCC because it acts with slow kinetics and a relatively high activation threshold (-30mV). On the other hand, $Ca_v1.3$ is defined by fast kinetics and a relatively low activation threshold (-55mV; Lipscombe et al., 2004). The greater sensitivity of $Ca_v1.3$ change in voltage is shown in Fig. 7C. This is remarkable considering $Ca_v1.2$ and $Ca_v1.3$ differ only in their α-1 pore subunit. Thus, with increased sensitivity to membrane polarization and faster-acting responses, $Ca_v1.3$ likely plays a more critical role in Ca^{2+} mechanics in the OHC.

A.

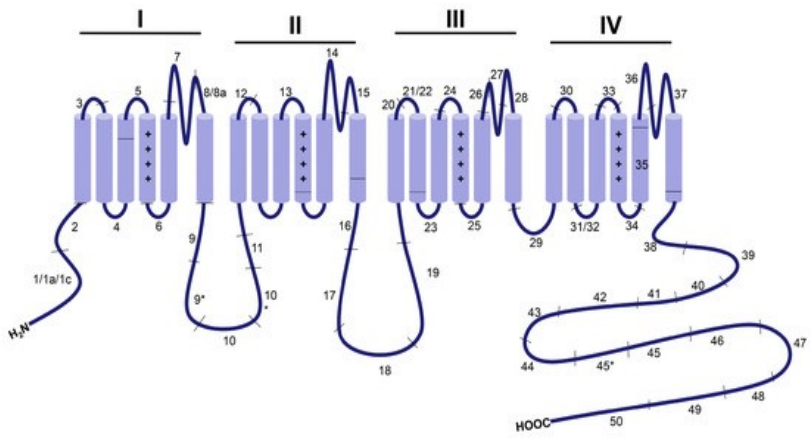

B.

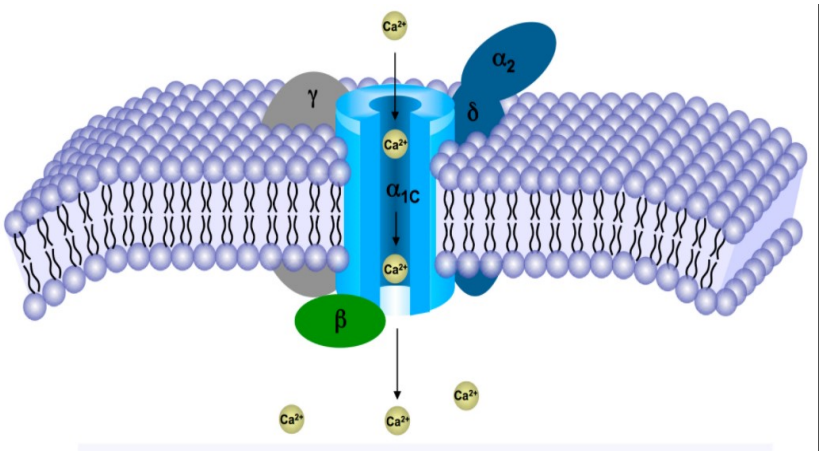

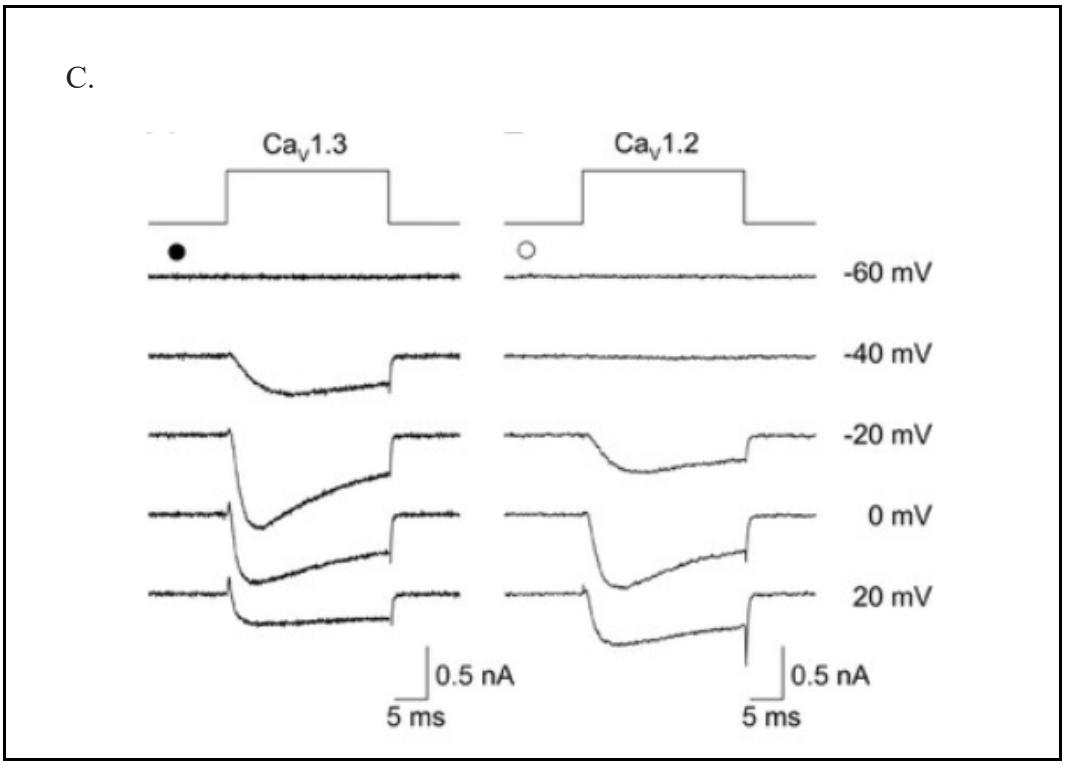

Figure 7**.** A-B) Diagrams of $Ca_v1.2$ and $Ca_v1.3$ structures, taken from Hu et al (2017). Their structures differ only at the α -1 site, labeled here as α-1C. C) Data from Lipscombe et al. (2004) demonstrating the low threshold sensitivity of $Ca_v1.3$ compared to $Ca_v1.2$. Currents were activated by step depolarizations to the indicated test potentials from a holding potential of −100 mV; 2 mM Ca^{2+} was the charge carrier.

$Ca_v1.2$ and $Ca_v1.3$ are not the only channels involved with extracellular Ca^{2+} influx. The ionotropic purinergic receptors **P2X2, P2X3,** and **P2X7** are found along the OHC and stereocilia membranes. They are stimulated by ATP-binding to open their pores to extracellular cations, augmenting the depolarization response in the OHC. P2X receptors consist of 3 subunits, each of which possesses transmembrane segments TM1 and TM2 and extracellular lysine (+) residues that contribute to ATP (-) binding (North et al., 2002; Fig. 8). 3 ATP molecules bind to the extracellular loops of the P2X receptor with the help of Zn^{2+}, which causes a conformational change in the protein that opens the

cation-specific pore to enable Ca^{2+} influx (Jiang et al., 2003; Nagaya el al., 2005). Their pores are not specific for particular cations but nonetheless enable extracellular Ca^{2+} to enter the cell down a concentration gradient (Housley et al., 1992). Patch-clamp tests by Skellet et al. (1997) showed 5-10 μM ATP is enough to induce P2X-mediated Ca^{2+} influx into OHCs. While this class of purinergic receptors is often found in homomeric form, they have the ability to assume heteromeric forms, such as P2X2/3. P2X7, however, exists only in homomeric form. Studies by Cockayne et al. (2005) showed that 90% of P2X2/3 heterotrimer knockouts died prematurely, suggesting an essential role for this heterotrimer systemically. It remains to be seen if the P2X2/3 heterotrimer plays a role in audition.

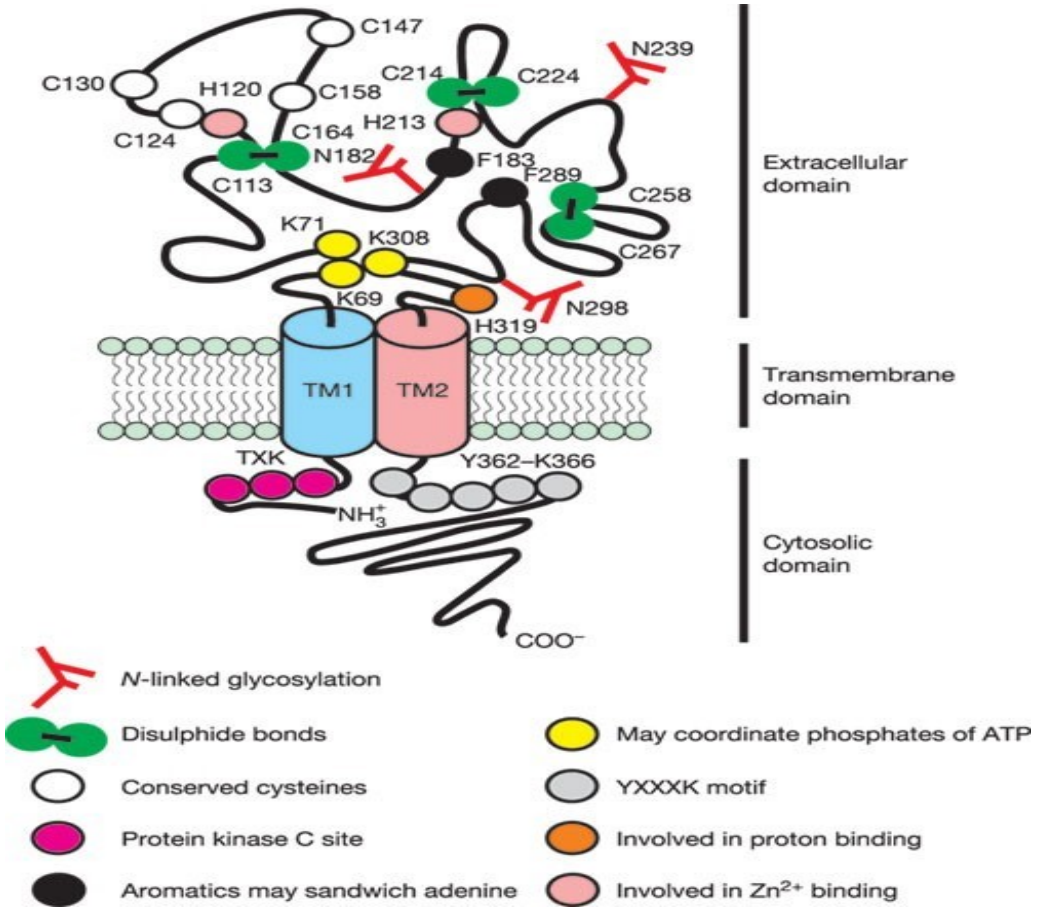

Figure 8. Diagram of a rodent P2X receptor subunit (Khakh and North, 2006).

P2X2, P2X3, and P2X7 differ in structure, location, and kinetics. Structural differences are the result of varying lengths of subunit amino acid chains. In adult P2 mice, P2X7 localizes weakly to the base of the OHC while P2X2 localizes to the apical OHC (Khakh and North, 2006). Kinetically, P2X2 activates more slowly P2X3 and P2X7 (Roberts et al., 2006). Activation of voltage-gated and ATP-gated channels create an

influx of Ca^{2+} that, in unison with $Ca_v1.2$ and $Ca_v1.3$, cause CICR and a robust influx of Ca^{2+} into the HC. The [Ca^{2+}] in the OHC during depolarization reaches ~ 240 nM (Szücs et al., 2004).

A transmembrane protein involved with the restoration of the OHC resting membrane potential is the plasma membrane Ca^{2+} ATPase, or **PMCA2**. It too, is involved with Ca^{2+} regulation. This pump, located on the membranes of stereocilia, uses 1 ATP to pump 1 Ca^{2+} out of the cell against an electrochemical gradient with a turnover rate of about 200 Ca^{2+} ions/second (Dumont et al., 2001; Chen et al., 2012). The PMCA2 ATP binding site is intracellular and relies upon phosphyl-aspartate (D*) and lysine (K) for binding capabilities. Its ability to bind and extrude Ca^{2+} from OHC stereocilia is greatly enhanced by interactions with calmodulin, which are catalyzed by phosphorylation by ATP (Carafoli, 1991; Albers and Siegel, 1999). Null mutations of the *Atp2b2* gene, coding for the PMCA2 pump isoform, are linked to hereditary deafness in both humans (Ficarella et al., 2007) and mice (Kozel et al., 1998; McCullough et al., 2004).

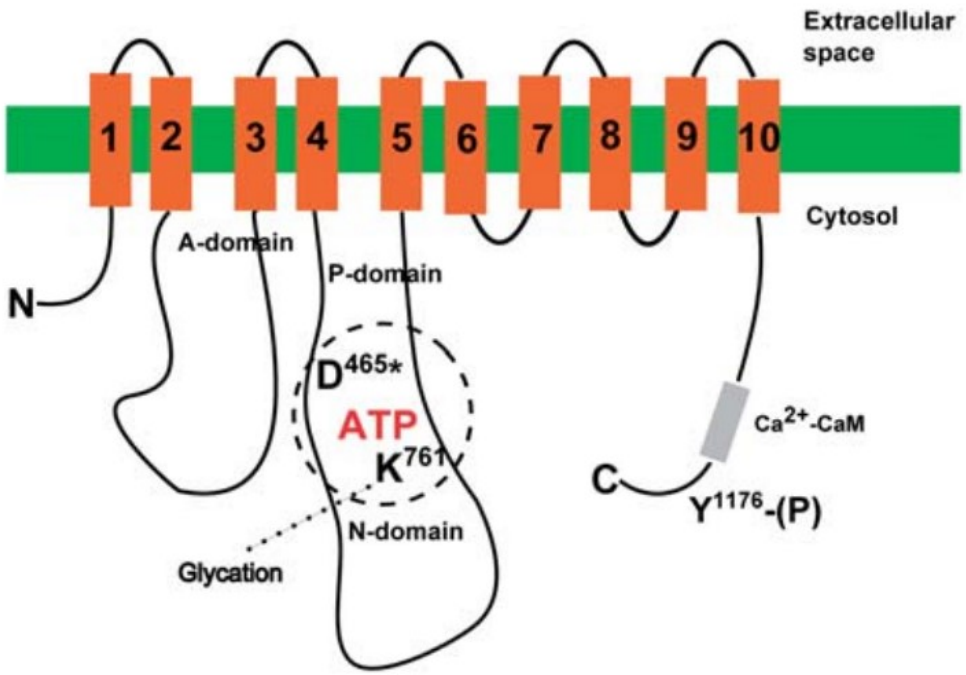

Figure 9. Simplified PMCA2 structure, taken from Horakova et al. (2013). The ATP binding site is intracellular and relies upon phosphyl-aspartate (D*) and lysine (K) for binding capabilities. The metabolism of 1 ATP molecule causes the extrusion of 1 Ca^{2+} ion.

Another protein associated with the OHC cell membrane is **prestin,** a motor protein localized to the lateral walls of OHCs that gives electromotile and amplifying properties to OHCs (Fig. 10; Tables 1-2; Liberman et al., 2002). Prestin uses a complex mechanism to elongate and contract itself, and since it is in the lateral OHC membrane, its movements elongate and contract the OHC, too. Thus, prestin is directly responsible for OHC electromotility, which is directly coupled to cochlear amplification (Liberman et al., 2002). Recent studies by the Simmons lab suggest that OCM and prestin interact in ways that promote the efficacy of the OHC. Prestin was not examined in this project, but its role in OHC function cannot be forgotten.

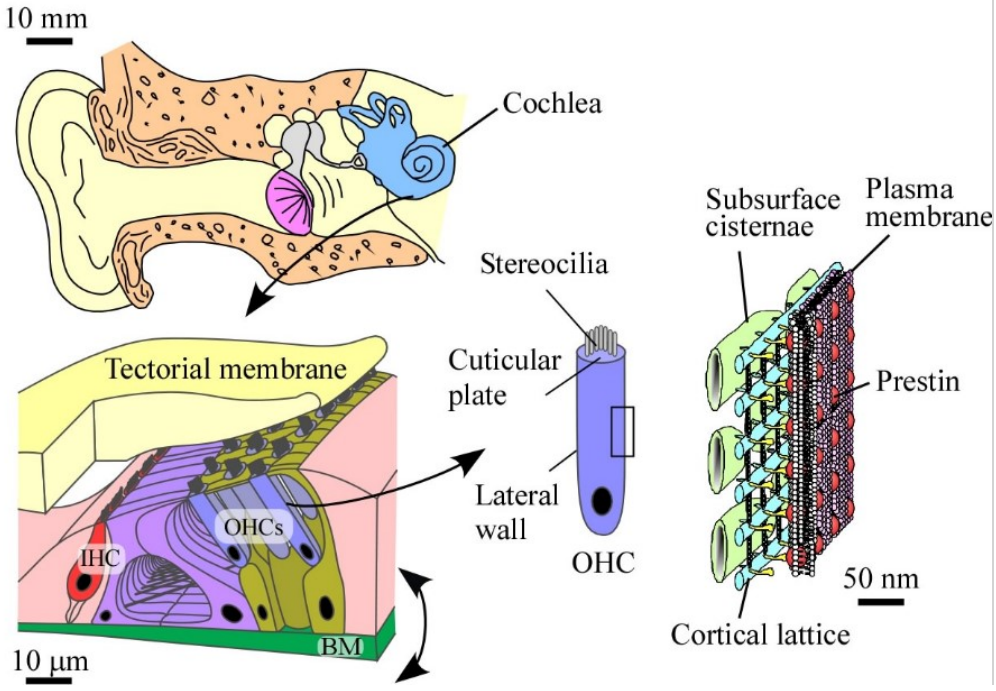

Figure 10: Prestin location and structure. A) Image describing prestin location, taken from the WADA Laboratory at Tohuku University.

Since Ca^{2+} regulators on the membrane of the OHC and stereocilia have been discussed, OHC CaBPs that serve as intracellular Ca^{2+} sensors/buffers. The OHC has several cytosolic CaBPs whose roles in hearing loss have been examined in other studies (Pauls et al., 1996; Schwaller et al., 2002; Schwaller, 2009, 2010, 2014; Permyakov et al., 2017). This study, however, examines two EF-hand proteins: alpha-parvalbumin (**aPV**) and beta-parvalbumin (**OCM)**. Like other EF-hand proteins, aPV and OCM Ca^{2+}-binding sites are helix-loop-helix motifs featuring negatively charged glutamate and aspartate, which create a net negative charge that attracts the positive charge of Ca^{2+} (Climer et al., 2019). As a result of their marked Ca^{2+}-binding ability, proteins within the EF-hand

family can serve as Ca^{2+} sensors, buffers, or both. The role of a Ca^{2+} sensor is to activate regulatory pathways upon binding free Ca^{2+}. The role of a Ca^{2+} buffer, on the other hand, is to bind free intracellular Ca^{2+} to control the intracellular [Ca^{2+}]. Ca^{2+} buffers ensure that excess Ca^{2+} does not induce reactive oxygen species formation, which can accumulate when intracellular Ca^{2+} reaches damaging levels and lead to cell death.

aPV is a mobile Ca^{2+} sensor in many tissues, but this study focuses on its role in OHC cytoplasm. It has two divalent helix-loop-helix binding domains specific for Ca^{2+}. Immunogold labeling experiments by Hackney et al (2005) demonstrated that aPV is expressed in both IHCs and OHCs, though more so in IHCs. Immunohistochemistry experiments by Simmons et al. (2010) showed that aPV expression declines with age in the OHC but rises in IHCs during neonatal development. (Dechesne et al., 1991, 1994; Pack and Slepecky, 1995; Soto-Prior et al., 1995; Schwaller et al., 2002; Yang et al., 2004; Schwaller, 2009, 2010, 2014). After birth, aPV's expression in IHCs increases and diminishes in OHCs by P6 (Simmons et al, 2010; Climer et al, 2019).

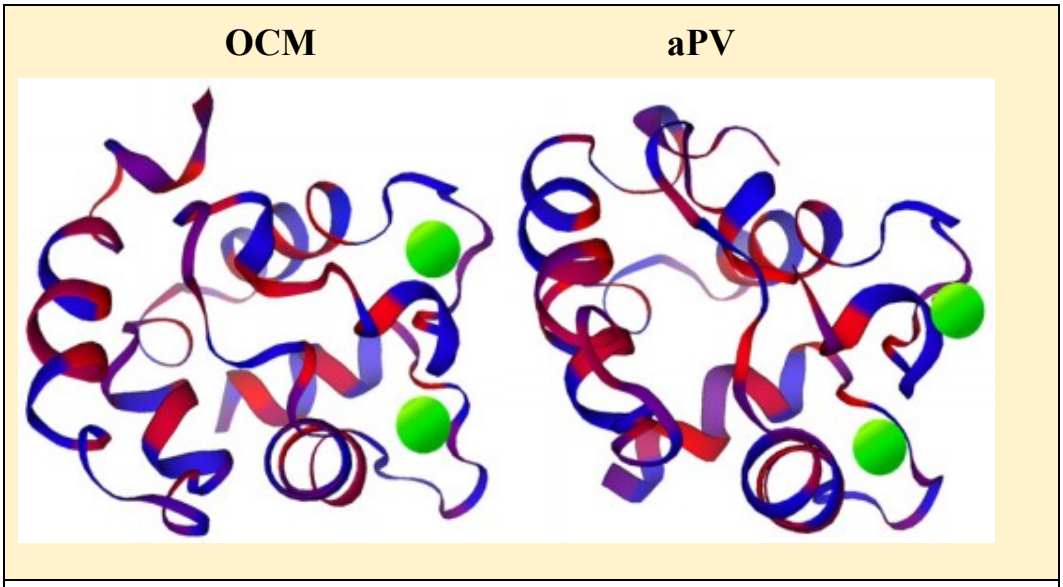

Figure 11. Ocm (left) and aPV (right) structure. Image taken from the Protein Database—Europe via Uniprot.org. Green spheres represent Ca^{2+} ions.

OCM shares 53% sequence homology with aPV (Berchtold, 1989). In fact, it has traditionally been referred to as beta-parvalbumin, yet a recent phylogenic analysis suggests it is not as closely related to aPV or even the beta-parvalbumin family as previously thought, which implies that OCM has evolved into a new category of parvalbumin proteins (Climer, et al., 2019). OCM differs from aPV in its affinity for Ca^{2+}, its isoelectric point, and C-terminal helix length (Goodman and Pechére, 1977; Hapak et al., 1989; Cox et al., 1990; Moncrief et al., 1990). OCM has one helix-loop-helix binding domain that specializes in binding Ca^{2+} and another capable of binding both Ca^{2+} and Mg^{2+}. Immunogold labeling experiments have shown that OCM is responsible for most of the Ca^{2+}-binding sites in the OHC, suggesting its role as a major modulator of intracellular Ca^{2+} in the OHC during mechanotransduction (Sakaguchi et al., 1998; Hackney et al., 2003; Hackney et al, 2005). OCM is found within the OHC cytosol but is

preferentially localized to the lateral membrane, cuticular plate, and basal pole opposite the efferent terminals (Simmons et al., 2010). Such localization could suggest that OCM plays a role in cochlear amplification and mechanotransduction. In the OHC, it is present at 2 to 3 mM in the apical region and at 969 μM in stereocilia (Hackney et al., 2005).

Since EF-hands are particularly good at binding Ca^{2+}, aPV and OCM are likely implicated in OHC Ca^{2+}-regulating pathways. OCM is of particular interest for several reasons. First, "knocking out" OCM from mice (*Ocm* KO mice) results in progressive hearing loss from 1-3 months and deafness by 4 months (Tong et al., 2016). Distortion product otoacoustic emissions (DPOAE), a test used to measure the functionality of OHCs, produced elevated hearing thresholds for *Ocm* KO mice. In other words, the threshold noise level needed to induce OHC responses was markedly increased in the absence of OCM. Thus, OCM has been shown to be involved the maintenance of OHC efficacy. Second, research has shown OCM to be a major contributor of OHC intracellular Ca^{2+}-binding sites (Hackney et al., 2005). Third, little is known about how OCM interacts with or within Ca^{2+}-regulating pathways. One way to illuminate what OCM is doing in OHCs is to examine the relationships between OCM and other important Ca^{2+} regulators through gene/protein expression analyses.

Table 3. Target gene and protein information.

Protein	Gene	Age of Protein Expression in Neonatal Murine Cochlea
OCM	*Ocm*	P2-3
aPV	*Pvalb*	P0
Prestin	*Slc26a5*	P6
PMCA2	*Atp2b2*	P0
P2X2	*P2rx2*	P1-2
P2X3	*P2rx3*	P1-2
P2X7	*P2rx7*	P1-2
$Ca_v1.2$	*Cacna1c*	P0
$Ca_v1.3$	*Cacna1d*	P0
Hearing Onset		P12

CHAPTER TWO

Methods and Materials

2.1 Generation of Ocm KO; GCamp6+s; Atoh-1-Cre^{+} mice

Ocm KO mice were created by cloning 17 kilobases of the *Ocm* gene (found on exons 2-4). A LoxP site was engineered on the 5' end of exon 2 and an Flp-neo-Flp-LoxP cassette eas engineered on the 3' end of exon 4 (Tong et al., 2016). The conditional KO mouse was first created in C57/Bl6 mice and then transferred to CBA mice. Spontaneous germline transmission occurred, and the deletion was transferred to the CBA/CaJ mouse genetic background for this project.

Ocm KO mice were crossed with the Ca^{2+} reporter mouse, GCaMP6s (Jackson Labs), which has a LoxP site flanked stop codon preventing expression. *Ocm* WT and KO mice carrying the GCaMP6s$^{F/F}$ allele were crossed with Atoh1-driven Cre mice to induce conditional expression GCaMP6s in the inner ear region. Genotyping results show all offspring express GCaMP while nearly half of them express Cre. Cre-positive mice were used for the following experiments. Cre negative mice were used as controls. *Ocm* KO mice show signs of hearing loss at 1-2 months and are essentially deaf by 4 months.

2.2 Cochlear Spiral Dissection

Dissections were completed under a dissecting microscope at room temperature (18°C). Neonatal mice (P0-P6) were obtained from the Baylor University vivarium, were sedated on ice, and euthanized by decapitation. The objective of the dissection was to remove the spiral of epithelium containing the organ of Corti from the bony labyrinth in the temporal lobe.

Starting from the newly-created opening on the caudal aspect of the cranium, small scissors were used to make a superficial midsagittal cut below the fur and across the top of the mouse's head until the incision was just posterior to the orbit. Starting at the anterior end of this midsagittal cut, a frontal cut was made below the fur just anterior to both ears. From a superior view, the final product was a T-shaped incision below the fur. Forceps were used to remove the fur created by the incision. With the fur removed from the cranium, the sample was placed in a small dish of Gibco™ 1x Hank's Balanced Salt Solution (+ Ca^{2+} / + Mg^{2+}) for subsequent steps.

The same T-shaped pattern was cut into the cranium, exposing the brain. The brain was removed by forceps and the two cochleae were visualized in the inferior temporal region. The cochleae were removed from the temporal lobe with the vestibular organs by using forceps to tear the cochlear-vestibular unit away from the temporal bone at the epiphyseal plates. Next, cochleae were separated from vestibular organs, its bulla was removed, and the interior spiral of sensory epithelia was separated from the greater epithelial ridge, thereby isolating the HCs, supporting cells, and basilar membrane from the rest of the surrounding tissue. This "spiral" was obtained from each cochlea (two per

animal) and was subjected to immunohistochemical and RT-qPCR analyses (discussed below).

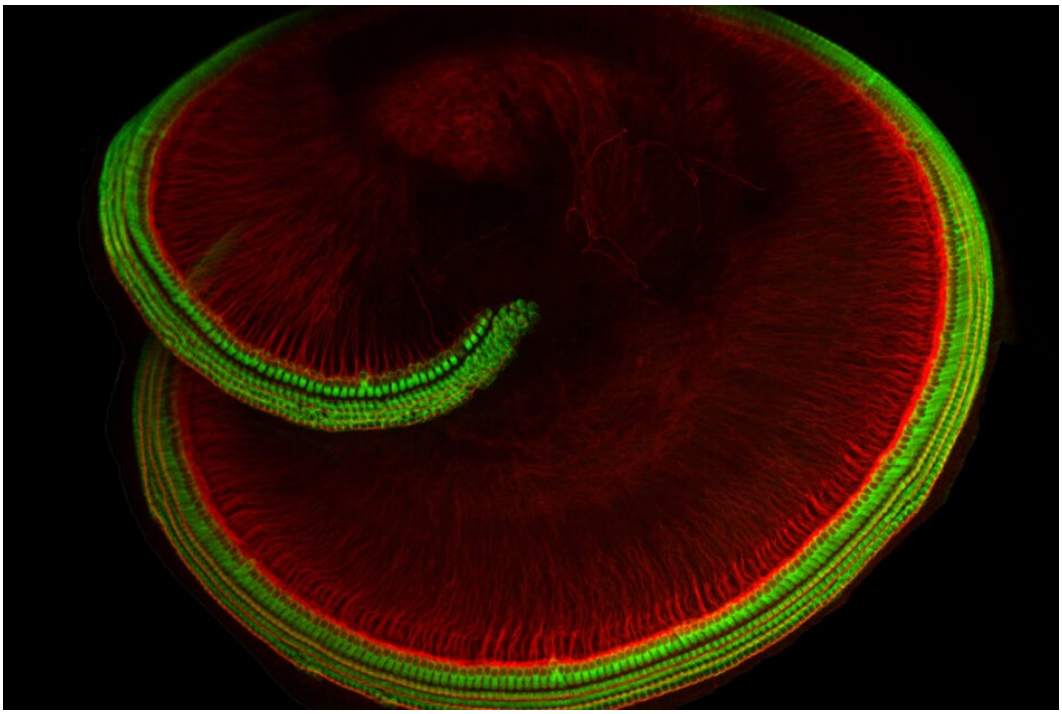

Figure 12. An example of a dissected spiral of cochlear sensory epithelium. Immunohistochemistry image demonstrating HC location along the spiral. Green fluorescence marks HCs. Red fluorescence marks neurons. Image taken from Harvard Holt lab, published in The Harvard Gazette.

If samples were not immediately tested, they were flash frozen in liquid nitrogen and stored at -80°C for up to 1 week. RNaseZap spray was used to clean the dissection station to impede RNase degradation.

2.3 Immunohistochemistry

Discussed in this section is the immunohistochemistry protocol used for P0-P6 mice.

1. Fixation
    a. Spirals were clipped at their basal region to ensure that the spiral lay down flat under the coverslip when placed on the microscope slide.
    b. Once cleaned and clipped, the spirals were placed into an upside-down, 1.5 mL tube cap and fixed in 200 uL of 4% paraformaldehyde for ≥ 45 minutes.
    c. Still in the cap, the sample was then rinsed 3 times with 200 uL of 1 x phosphate buffered saline (PBS) by simply pipetting the 4% paraformaldehyde out, adding the 1 x PBS, removing the 1 x PBS, and repeating the rinse 2 more times (for a total of 3 rinses). If the procedure could not be completed that day, the sample was left at this step (in 1 x PBS) at 4°C for up to 3 days without effect.
2. Block
    a. The rinsed sample was then placed in a 5% natural horse serum-triton solution (NHS-T; 0.3% Triton X-100) for 1 hour on a laboratory shaker. NHS blocks non-specific binding while Triton permeabilizes cells, allowing the exogenous antibodies to flood the cell and bind specifically to the target antigen.

b. The blocked sample was rinsed 3 times for 10 minutes (4, 3, and 3 minutes) with PBS on a laboratory shaker. The sample was then ready for primary antibody administration.

3. Primary antibody administration
    a. Primary antibodies, stored at 4 °C, were diluted on ice to meet the predetermined antibody working concentrations (Table 4). Stock antibody was diluted with 1% NHS.
    b. With the samples in the upside-down tube caps, antibodies were gently applied under a dissecting microscope using a micropipette.
    c. Once antibodies were administered to their sample, the tubes were placed on the upside-down tube caps. The result was an upside down 1.5 mL tube with the antibody solution/sample sitting int the cap. The total solution volume was 100 µL per sample.
    d. The samples (still in their solution) were immediately placed in a 37°C oven for overnight storage.
4. Secondary antibody administration
    a. The samples were removed from the oven and rinsed 3x in PBS.
    b. Secondary antibodies, diluted in 1% NHS, were applied to the sample in amounts that would achieve the desired working concentration (Table 5). The total solution volume was 100 µL per sample.
    c. Samples, now in their secondary antibody solution, were placed in the 37°C oven for 1 hour.

d. Samples were rinsed 3x with PBS.

5. Mounting
    a. Samples were mounted under a dissecting microscope. A drop of VECTASHIELD mounting medium (for fluorescence with 4′,6-diamidino-2-phenylindole (DAPI)) was placed on a clear slide.
    b. The sample was carefully placed in the mounting medium. It was important to lay the cochlear spiral flat to prevent it from folding over itself, which would hinder microscopic fluorescence imaging.
    c. A coverslip was placed over the sample.
    d. The slides were moved into a Fisher slide warmer until the coverslip adherent had dried.
6. Imaging was completed using confocal microscopy and Zen software by Zeiss which enabled the user to simultaneously take laser images and analyze them on a nearby desktop. This experiment utilized green, far red, red, and blue laser channels.

Table 4. Primary antibody information. Antibodies from the same animal (donkey or goat; blue or orange) were not applied to the same sample. For example, anti-OCM and anti-P2X2 was a compatible antibody combination, but not anti-OCM and anti-aPV.

Primary Antibodies			
Antibody Name	Source	Host	Working Concentration
Anti-Oncomodulin	SWANT	Goat	1:200
Anti-aPV	SWANT	Goat	1:200
Anti-P2X2	Protein Tech Grp.	Rabbit	1:400
Anti-P2X3	Protein Tech Grp.	Rabbit	1:400
Anti-P2X7	Protein Tech Grp.	Rabbit	1:400

Table 5. Secondary antibody information.

Secondary Antibody Information			
Antibody Name	Source	Host	Working Concentration
Alexa Fluor 546 Donkey anti-Rabbit IgG (H+L) Secondary Antibody	Life Technologies	Donkey anti rabbit	1:200
Northern Lights dk a gt 637	R&D Systems	Donkey anti goat	1:200
DAPI (stains blue)	Vector Laboratories, Inc.	N/A	N/A

2.4 RNA Extraction and Purification

RNA was extracted and purified from samples using the *Qiagen RNeasy Plus Micro Kit: Purification of Total RNA from Animal and Human Tissues*. Filtered Eppendorf pipette tips were used and the procedure was conducted at room temperature (18°C). RNaseZap spray was used consistently throughout the experiment.

1. Spirals were homogenized in 350 uL RLT buffer + beta-mercaptoethanol (1%), at room temperature, in a 2 mL tube by vortexing until spirals were no longer visible, or no longer intact. Two spirals (n=2) were homogenized in every tube.
2. Tubes with homogenized spirals were centrifuged at 16,000 rpm for 3 minutes.
3. Lysate was collected and transferred into the gDNA Eliminator Column, which was then centrifuged at 10,000 rpm for 1 minute.
4. After removing the filter, 350 uL of 50% ethanol was added to the flowthrough of each tube. This 700 uL solution was added to a RNeasy MinElute Spin Column (stored at 4°C but used at 18°C).
5. The spin column was centrifuged at 12,000 rpm for 20 seconds. Flowthrough discarded.
6. 700 uL RW1 was added to each tube then centrifuged at 12,000 rpm for 20 seconds. Flowthrough discarded.
7. 500 uL RPE was added to each tube then centrifuged at 12,000 rpm for 20 seconds. Flowthrough discarded.
8. 500 uL 80% EtOH was added to each tube then centrifuged at 12,000 rpm for 2 minutes. Flowthrough discarded with the collection tube.

9. The MinElute filter cartridge was placed in a new collection tube, its cap was left open, and then was centrifuged at 14,800 rpm for 5 minutes. This step ensures removal of EtOH from the filter membrane which can hinder RNA purity. The tube and its EtOH was discarded.
10. The MinElute filter cartridge was placed in a new 2 uL collection tube and 14 uL of nuclease-free water was placed gently on the filter membrane. The tube was then centrifuged at 16,000 for 1.5 minutes.
11. RNA quantity (ng/uL) and quality (260/280; 260/230) were determined using a Nanodrop spectrophotometer. RNA concentrations were normally in the 8-15 ng/uL range. 260/280 values were normally between 1.8 and 2.0. 260/230 values were normally substandard due to the presence of ethanol, but it is possible that the ethanol evaporated when exposed to high temperatures during cDNA synthesis.
12. If RNA was not immediately reverse transcribed to complementary DNA (cDNA), tubes were stored at -80°C for up to 2 weeks.

2.5 Primer Design

Primers for gene targets were obtained in 1 of 3 ways: 1) primers were designed using the NCBI primer design and BLAST tools, 2) primers were found in published journal articles, 3) primers were found on an online database, the Harvard Primer Bank (Wang and Seed, 2003; Spandidos et at., 2008; Spandidos et at., 2010; Wang et al., 2012). Upon arrival, primers were tested with standard curve analysis and were optimized

by running a temperature gradient RT-qPCR to determine which annealing temperature enabled optimal amplification. The annealing temperature used for all reactions was 60°C. The primers and their sequences are listed below in Table 3.

Table **6.** RT-qPCR primer information.

Primer Target	Sequence (5' → 3')
OCM	F: ATGAGCATCACGGACATTCTGAGC R: CTGGCAGACATCTTGGAGAGGC
aPV	F: GACTCCTTCGACCACAAAAAG R: ATCCTCCTCAATGAAGCCAC
PMCA2	F: GCTGCTGCTGCTGTTGTTTGA R: ATGGTTGAATGAAGGAGGGCAGGA
P2RX2	F: GCGTTCTGGGACTACGAGAC R: ACGTACCACACGAAGTAAAGC
P2RX3	F: CAGGGCACTTCTGTCTTTGTC R: CTCTTACTCCTCTTCATGGCGA
P2RX7	F: CCCTGCACAGTGAACGAGTA R: CGTGGAGAGATAGGGACAGC
$Ca_v1.2$	F: ATGGTCAATGAAAACACGA R: ACTGACGGTAGAGATGGTTG
$Ca_v1.3$	F: GCAAACTATGGCACCAGAC R: CTTTGGGAGAGAGATCCTACAGGTG
B2M	F: TGGTCTTTCTGGTGCTTGTC R: GGGTGGAACTGTGTTACGTAG

2.6 Reverse Transcription Quantitative Polymerase Chain Reaction (RT-qPCR)

Once the RNA was collected and purified, it was reverse transcribed to cDNA using the iScript Advanced cDNA Synthesis Kit for RT-qPCR. Reagents were kept on ice and filter tips were used. RNaseZap spray was used consistently throughout the experiment.

1. 0.5 uL PCR tubes were used for this reaction.
2. 5 uL of nuclease-free water was added to each PCR tube.
3. 4 uL of 5 x iScript Reaction Mix was added to each PCR tube.
4. 1 uL of iScript Reverse Transcriptase was added to each PCR tube.
5. 10 uL of RNA was added to each PCR tube.
6. Tubes were placed in Bio-Rad CFX96 C1000 Touch Thermal Cycler for 20 minutes at 46°C, 1 minute at 96°C, and infinity at 12°C.
7. Subsequently, cDNA was stored in -20°C for up to 1 month

With cDNA synthesis complete, RT-qPCR was ready to begin.

1. The RT-qPCR was conducted using filter tips and at room temperature (18°C) on the open bench top. Master mixes were made for each target gene, including the reference gene, beta-2-microglobulin (B2M) being analyzed according to the following ratio:

Table 7. RT-qPCR well set-up.

Reagent	Volume per well*
SsoAdvanced Universal SYBR Green Supermix	10 uL
Nuclease-free water	8.4 uL
Target Primer (forward)	0.3 uL of 10 uM
Target Primer (reverse)	0.3 uL of 10 uM
cDNA**	1 uL

*Volumes necessary to complete this reaction were multiplied by 1.05 to account for pipetting error.
**cDNA was NOT added to master mix solutions.

2. Master mixes were homogenized by pipette mixing.
3. The 96-well plate was filled first with the master mix (19 uL each well) and then the 1 uL of cDNA was added to each well individually to create a total reaction volume of 20 uL. The addition of cDNA well-by-well increased the uniformity of substrate for each reaction.
4. No template control wells were included for each target's master mix to ensure the absence of contamination.

5. The plate was sealed with an optically-clear plastic sheet, centrifuged for 20 seconds, and then placed into the Bio-Rad CFX96 C1000 Touch Thermal Cycler using the SsoAdvanced Universal SYBR Green Supermix RT-qPCR protocol.
    a. Amplification:
        - 96°C for 30 seconds
        - 98°C for 30 seconds
        - 72°C for 1 minute
        - 60°C for 30 seconds (annealing temperature)
        - fluorescence image recorded
        - steps (iv) and (v) were repeated 40 times for quantification.
    b. Melt Peak:
        - 72°C for 15 seconds
        - 96°C for 15 seconds
        - 12°C for infinite time
6. Amplification and melt peak data were recorded by the thermal cycler, downloaded onto a USB drive, and plugged into a computer capable of supporting the analysis software, CFX96 Manager, used to annotate and analyze the RT-qPCR run through fluorescence detection.

2.7 Statistical Analysis

Quantification values were determined using the $2^{-\Delta\Delta C_T}$ method, a mathematical formula that determines the relative fold difference in expression compared to a normalization group (Livak and Schmittgen, 2001). The group to which all data was normalized was P0 WT. B2M served as the housekeeping gene for each RT-qPCR run. A second housekeeping gene for each RT-qPCR run was not used because previous experiments in our lab using B2M and TBP (TATA-binding protein) were not significantly different from those only using B2M. Also, B2M had consistent and high levels of expression, which was optimal for relative quantification experiments. The $2^{-\Delta\Delta C_T}$ method is shown below in Fig. 13.

$$Ct_{B2M} - Ct_{target} = \Delta Ct_1$$

$$\Delta Ct_{normalizing\ group} - \Delta Ct_1 = \Delta\Delta Ct$$

$$2^{-\Delta\Delta Ct} = fold\ expression\ level$$

Figure 13. Equation used to determine the fold mRNA expression level. For example, a $2^{-\Delta\Delta CT}$ value of 3 means that the protein of interest has 3x more mRNA expression than the normalization control.

Quantification values were analyzed using Prism 8 for macOS (version 8.4.3 (471)). An unpaired t-test was used to determine whether subsets of data (by age and genotype) had statistically significant differences. Standard deviation was also calculated to account for variation in the RT-qPCR experiment.

CHAPTER THREE

Results

3.1 Loss of OCM reduces neonatal VGCC expression.

To determine the impact that OCM had on VGCC gene expression, RT-qPCR was used to obtain *Cacna1c* and *Cacna1d* mRNA expression in *Ocm* WT and KO mice. *Cacna1c* and *Cacna1d* were found to have decreased mRNA expression both in the absence of OCM and with age, as seen in Figure 13A. *Cacna1c* demonstrates significantly lower mRNA expression in *Ocm* KOs compared to *Ocm* WTs for ages P0 and P6. *Cacna1d*, on the other hand, demonstrates significantly lower mRNA expression in the absence of OCM only at age P0 (Fig. 13A). Generally, both *Cacna1c* and *Cacna1d* mRNA expression decline during maturation from P0 to P6 (Fig. 13B).

Immunohistochemistry experiments by Simmons et al. (2010) have shown OCM expression to occur at around P2-3 in murine OHCs. Approaching the onset of OCM at P2, *Ocm* WT mice demonstrate a substantial decrease in *Cacna1c* and *Cacna1d* mRNA expression relative to *Ocm* KO mice (Fig. 13B). This is interesting, because if OCM expression begins at P2, there should be no difference in *Cacna1c* mRNA expression between *Ocm* WT and *Ocm* KO at P0. Indeed, *Cacna1d* also experiences significantly different levels of mRNA expression between *Ocm* WT and KO mice before OCM expression begins. While VGCCs in *Ocm* KO mice experience a decline in mRNA expression with age, their rate of decline is slower than VGCCs in *Ocm* WT mice.

Ultimately, losing the *Ocm* gene reduces the early gene expression of *Cacna1c* and *Cacna1d.*

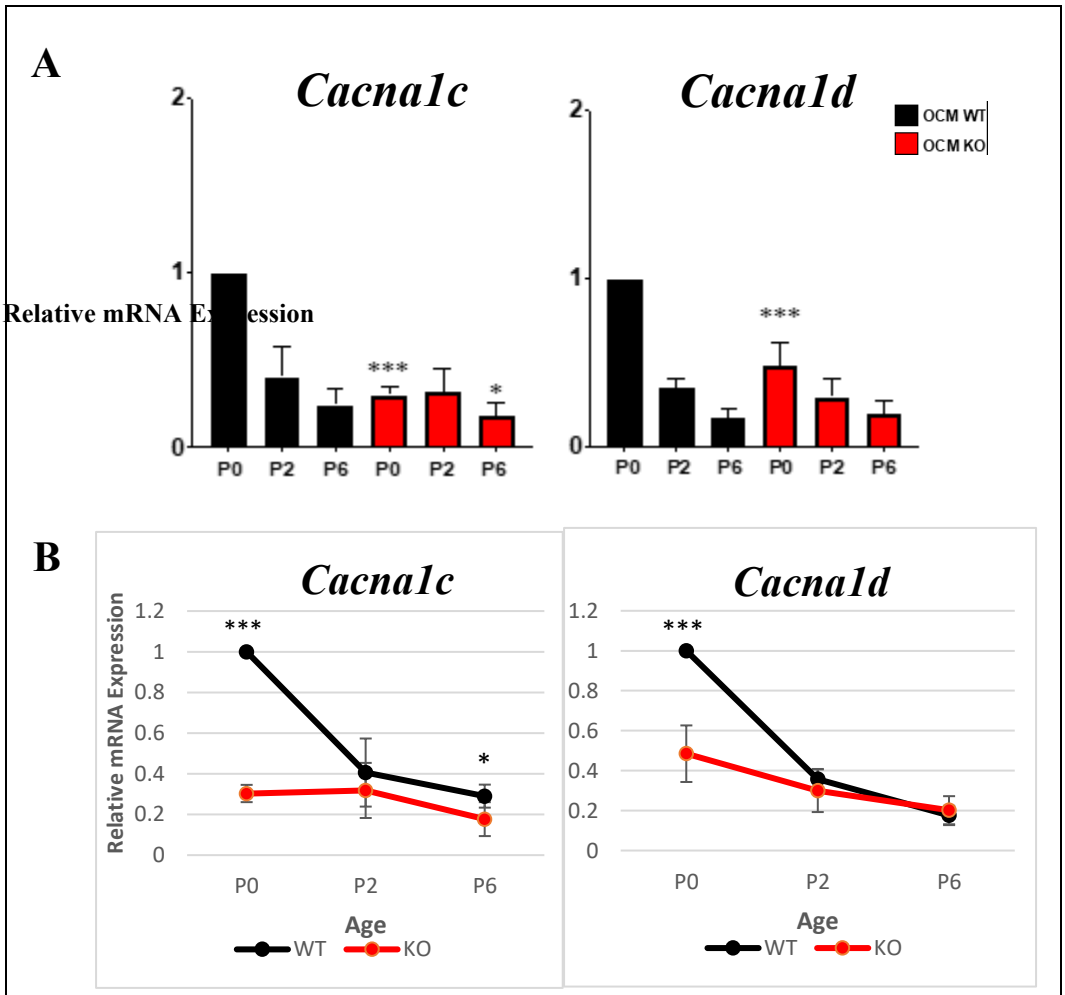

Figure 14. Relative gene expression for *Cacna1c* and *Cacna1d* in organ of Corti spirals from GCaMP6s+ mice at P0, P2, and P6. A) Targeted deletion of *Ocm* causes a general reduction in VGCC expression, particularly at P0. B) In both OCM WT and KO, *Cacna1c* and *Cacna1d* mRNA expression decreases with age. No significant differences in mRNA expression occur after the onset of OCM at P2. Plotted are the mean (± SD) mRNA levels normalized to P0 WT, which were determined using RT-qPCR. Asterisks (*) indicate a significant difference between WT and KO gene expression for the same age ($p < 0.05$, unpaired t-test). n = 2-4 for each group.

3.2 Loss of OCM causes a general upregulation of neonatal P2X expression.

Next, to determine whether OCM impacted P2X receptors, RT-qPCR was used to measure *P2rx2, P2rx3, and P2rx7* mRNA expression and immunohistochemistry to examine P2X2, P2X3, and P2X7 protein expression at P0, P2, and P6. Results were compared between *Ocm* WT and *Ocm* KO mice. RT-qPCR data suggests that purinergic receptors are generally upregulated in the absence of OCM (Fig. 15A). At P0 and P2, *P2rx2* mRNA expression is significantly greater in *Ocm* KO mice than in WT mice but falls below WT mice mRNA expression by P6. Similarly, *P2rx3* mRNA expression is greater in KO mice than in WT mice at P0 and P2 but demonstrates similar, declining expression by P6. *P2rx7* mRNA expression is significantly greater in KO mice than in WT mice only at P0, and its expression experiences a continuous decline from P0 to P6 (Fig. 15B)

Interestingly, when OCM protein expression turns on at P2-3, *P2rx2* mRNA begins to upregulate, suggesting a possible relationship between the expression of *Ocm/*OCM and *P2rx2*/P2X2. This is further evidenced the decline in *P2rx2* mRNA expression from P2-P6 in the absence of OCM (Fig. 15B). Both *P2rx3* and *P2rx7* in KO mice have high but falling mRNA expression between P0 and P2. By P6, their mRNA expression matches expression in WT mice.

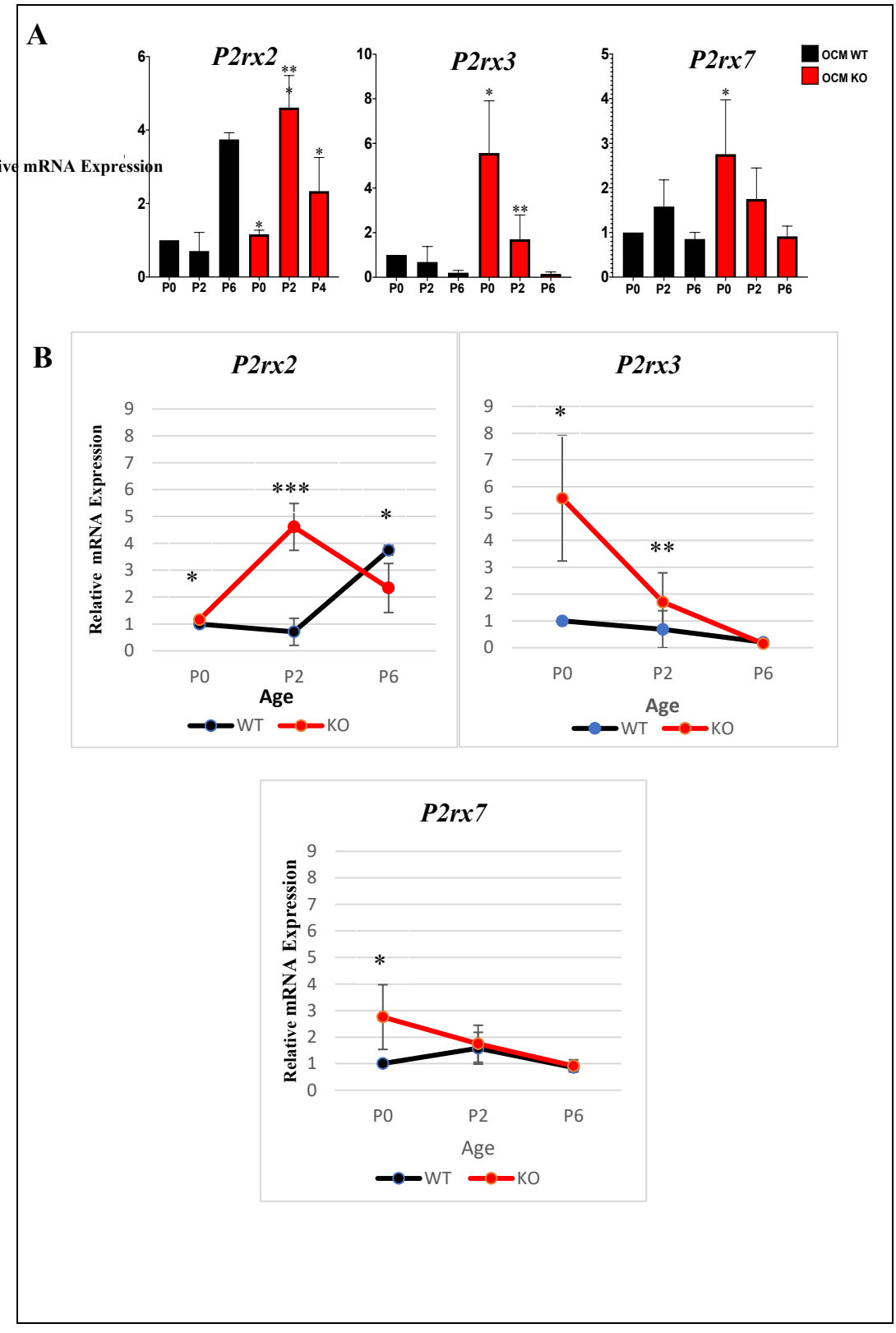
A
P2rx2
P2rx3
P2rx7
OCM WT
OCM KO
Relative mRNA Expression
P0 P2 P6 P0 P2 P4
P0 P2 P6 P0 P2 P6
P0 P2 P6 P0 P2 P6
B
P2rx2
P2rx3
P2rx7
Relative mRNA Expression
Age
WT
KO
P0
P2
P6

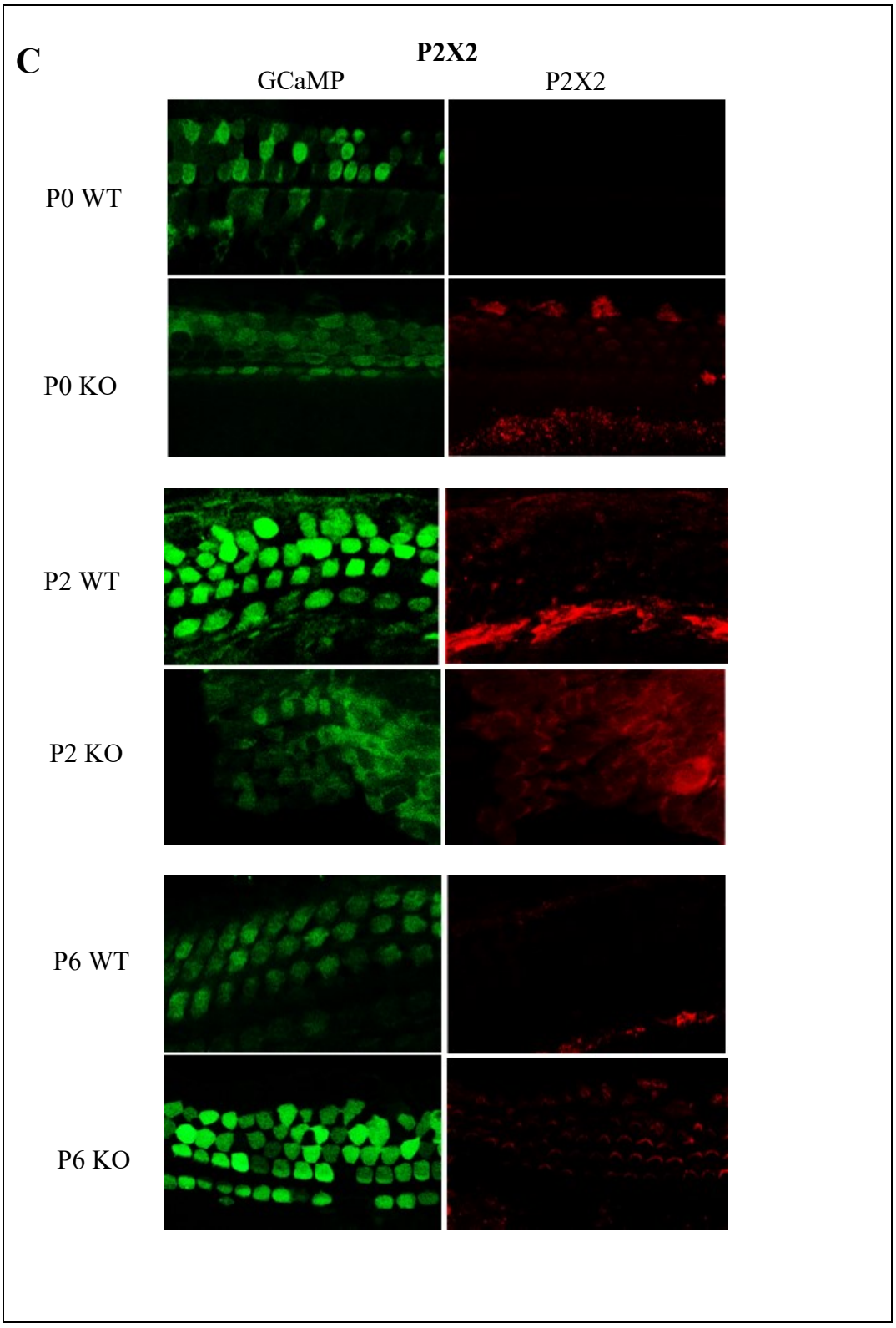
C
P2X2
GCaMP
P2X2
P0 WT
P0 KO
P2 WT
P2 KO
P6 WT
P6 KO

P2X3

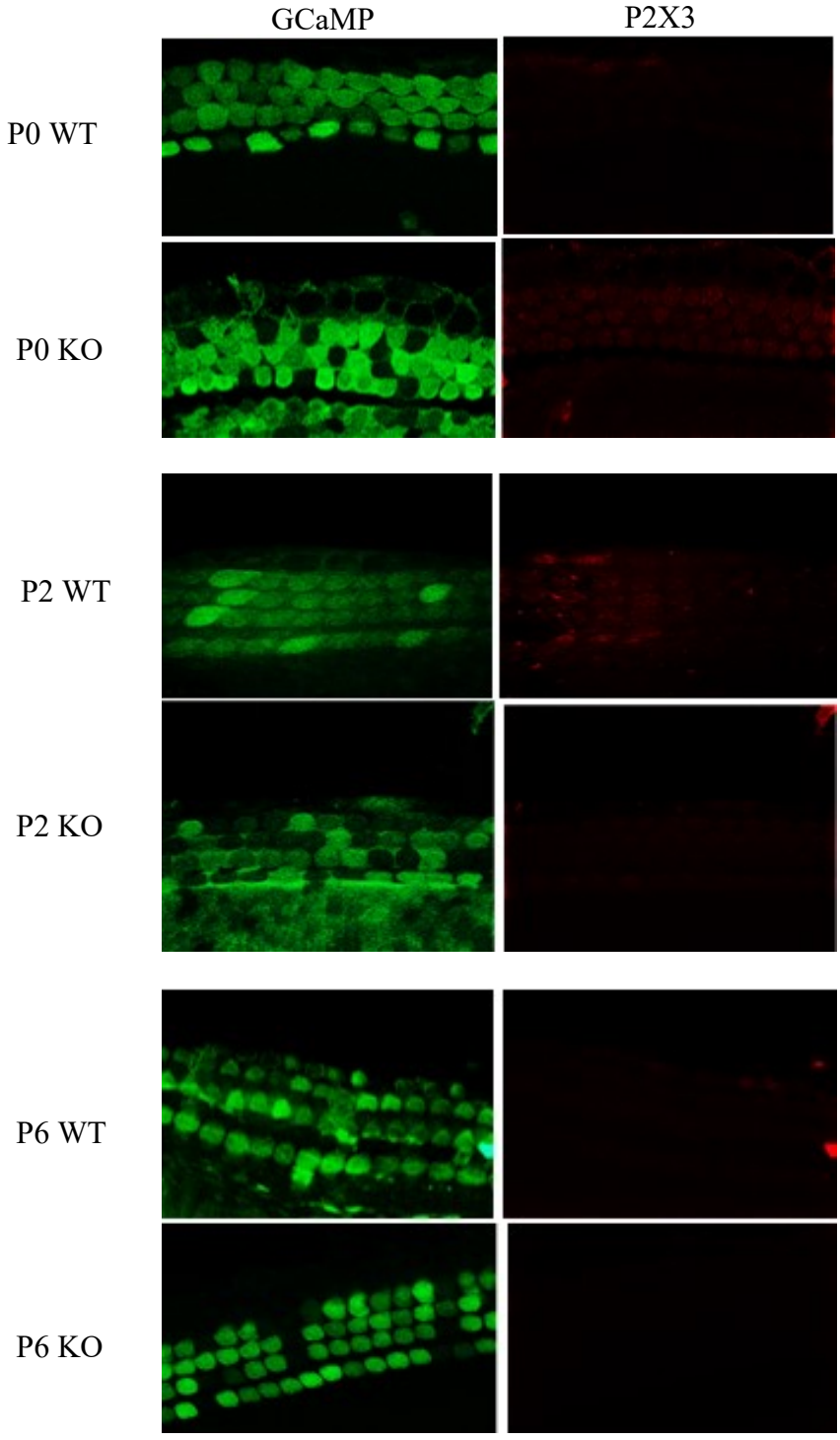

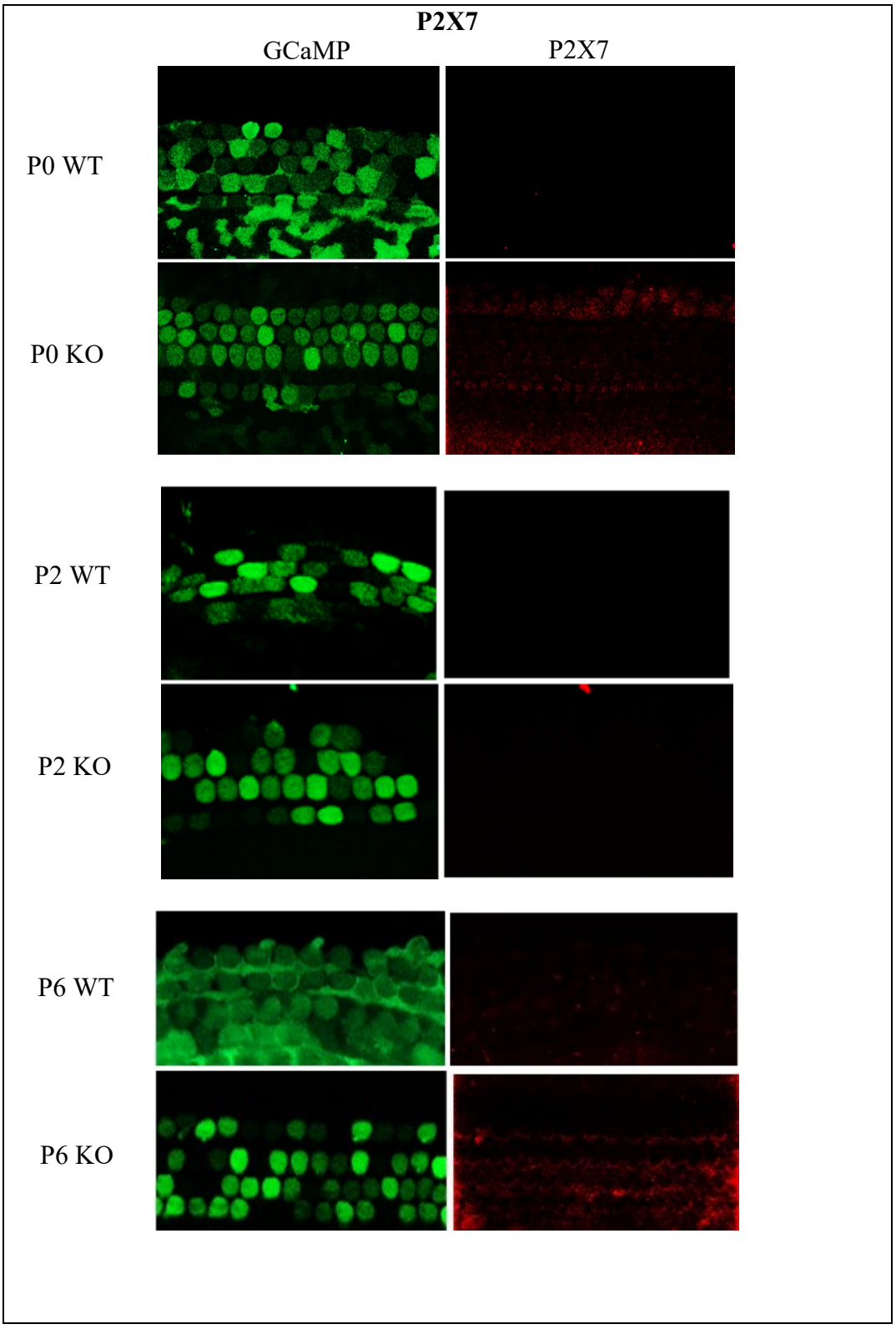
P2X7
GCaMP
P2X7
P0 WT
P0 KO
P2 WT
P2 KO
P6 WT
P6 KO

Figure 15. Relative gene expression for P2X2, P2X3, and P2X7 in Organ of Corti spirals from GCaMP6s+ mice at P0, P2, and P6. Plotted are the mean (± SD) mRNA levels normalized to P0 WT, which were determined using RT-qPCR. Asterisks (*) indicate a significant difference between WT and KO gene expression for the same age ($p < 0.05$, unpaired t-test). A-B) 2 different graphical representations of the same data that enable the viewer to see relative expression (A) and longitudinal expression more easily (B). n = 2-4 for each group. C) Immunohistochemistry images taken at 63x. Two aPV P6 images have been included for both WT and KO in order to show their expression at the subcuticular and supracuticular regions of the OHCs. Specifically, the supracuticular region OHCs show aPV localization to the stereocilia, especially in KO mice. Green channel represents GCaMP, a HC marker.

Immunohistochemistry complemented RT-qPCR data by showing upregulation of P2X2 in the absence of OCM. At P2, P2X2 expression in WT mice appears greater than in KO mice. However, most fluorescence in WT mice originates from the supporting cell region, not the OHCs. Immunolabeling P2X2 occurred in stereocilia of P2 and P6 KO mice.

Similar to RT-qPCR, immunohistochemistry showed that P0 P2X3 expression is greater in KO mice than WT mice. P2X3 labeling at P2 in the WT does not reflect data obtained from RT-qPCR. However, that does not mean that either is inaccurate. It is important to remember that mRNA levels do not always equate to protein levels, and vice versa.

Finally, immunohistochemistry showed a small (but significant) increase in P0 P2X7 expression in the absence of OCM. This finding aligns with RT-qPCR data, except in P6 KO mice where there was intense immunolabeling of P2X7 in OHC stereocilia.

3.3 Loss of OCM alters Atp2b2 mRNA expression.

Having shown that OCM regulates Ca^{2+} importer expression, attention turned toward an important Ca^{2+} exporter—PMCA2 (*Atp2b2*). *Atp2b2* mRNA expression was examined in WT and KO at ages P0, P2, and P6. Data showed that *Atp2b2* mRNA expression is altered in the absence of OCM (Fig. 16). P0 shows no significant difference between *Atp2b2* expression in *Ocm* WT and KO mice (Fig. 16A). At P2, however, *Atp2b2* mRNA expression falls in the absence of OCM. Because *Atp2b2* mRNA expression falls if OCM fails to turn on at P2, it is possible that OCM plays a role in *Atp2b2* gene regulation. Further, significantly greater *Atp2b2* mRNA expression was found in *Ocm* KO mice than in WT mice at P6—a time when OCM should already be buffering within the OHC.

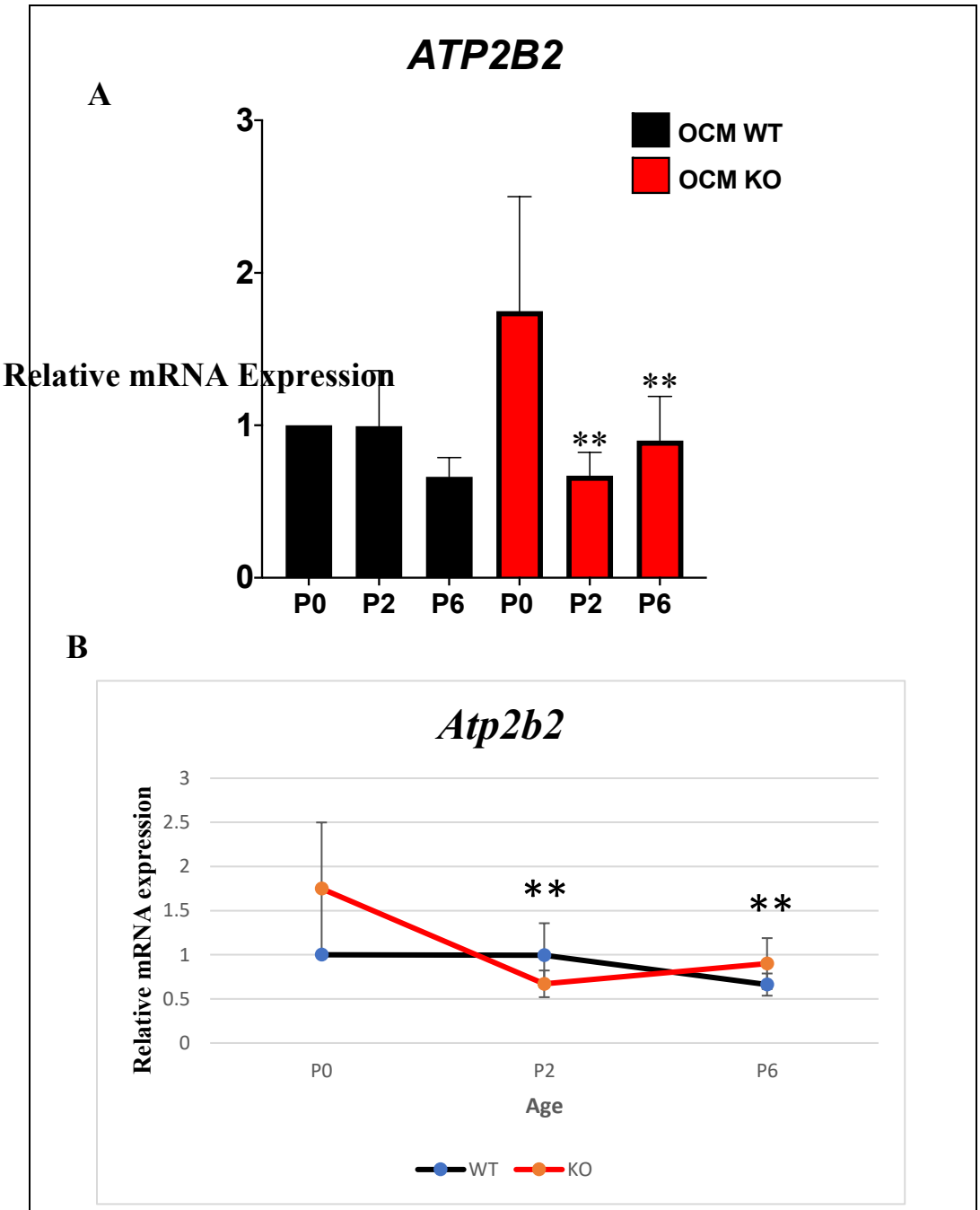

Figure 16. Relative gene expression for *Atp2b2* in Organ of Corti spirals from GCaMP6s+ mice at P0, P2, and P6. Plotted are the mean (± SD) mRNA levels normalized to P0 WT, which were determined using RT-qPCR. Asterisks (*) indicate a significant difference between WT and KO gene expression for the same age ($p < 0.05$, unpaired t-test). A-B are 2 different graphical representations of the same data that enable the viewer to see relative expression (A) and longitudinal expression more easily (B). n = 2-4 for each group.

3.4 aPV is downregulated in the absence of OCM.

Having seen the impact of OCM on Ca^{2+} importers and exporters, attention was turned toward aPV/*Pvalb*—an important cytosolic Ca^{2+} sensor in HCs. In *Ocm* KO mice, *Pvalb* experienced a significant downregulation in mRNA expression from P0-P6 in comparison to WT mice. While KO mice do show aPV immunolabeling, most of it is in the stereocilia. Both WT and KO mice showed marked aPV immunolabeling in stereocilia beginning at P2. aPV immunolabeling in cell bodies of OHCs occurred primarily in WT mice. The greater total aPV expression in WT mice (cell body + stereocilia) aligns with RT-qPCR findings (Fig. 17A).

RT-qPCR and immunohistochemistry data for OCM appear as expected—no mRNA or protein expression at P0, increasing amounts at P2, and large amounts at P6 (see Fig 16A/C). OCM KO mice displayed little to no indication of OCM mRNA or immunolabeling.

Fig. 17B demonstrates that, starting at P2, *Ocm* mRNA expression increases significantly. *Pvalb* mRNA expression, however, increases until P2—when OCM expression begins in the OHC—and then declines to nearly half its relative mRNA expression by P6. The reason for this is unknown. In *Ocm* KO mice, both *Ocm* and *Pvalb* mRNA expression do not experience a significant change during maturation. They both exist at very low levels.

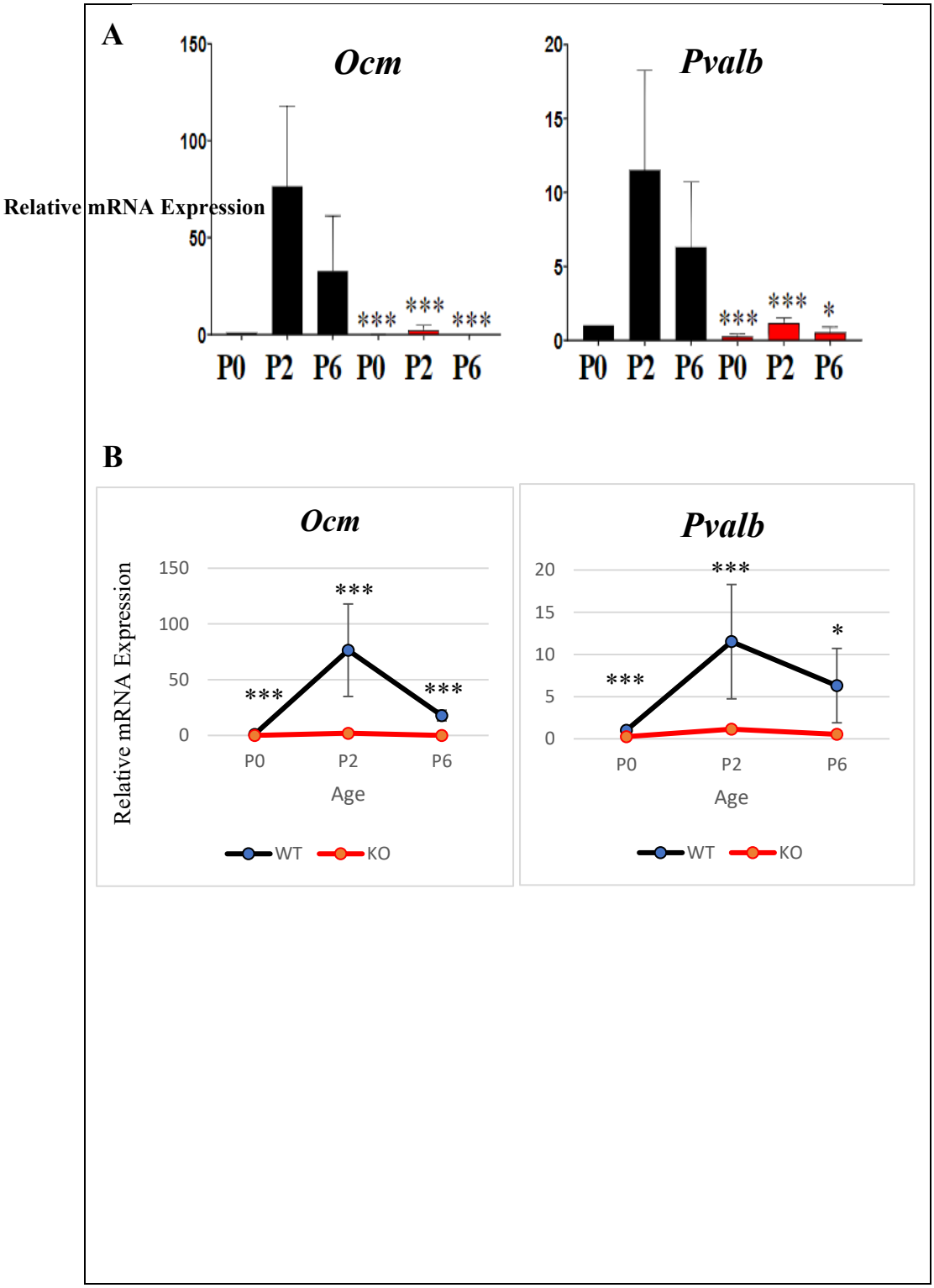
A
Ocm
Pvalb
Relative mRNA Expression
150
100
50
0
20
15
10
5
0
***
***
***
***
***
*
P0 P2 P6 P0 P2 P6
B
Ocm
Pvalb
Relative mRNA Expression
150
100
50
0
20
15
10
5
0
***
***
***
***
*
P0
P2
P6
Age
WT
KO

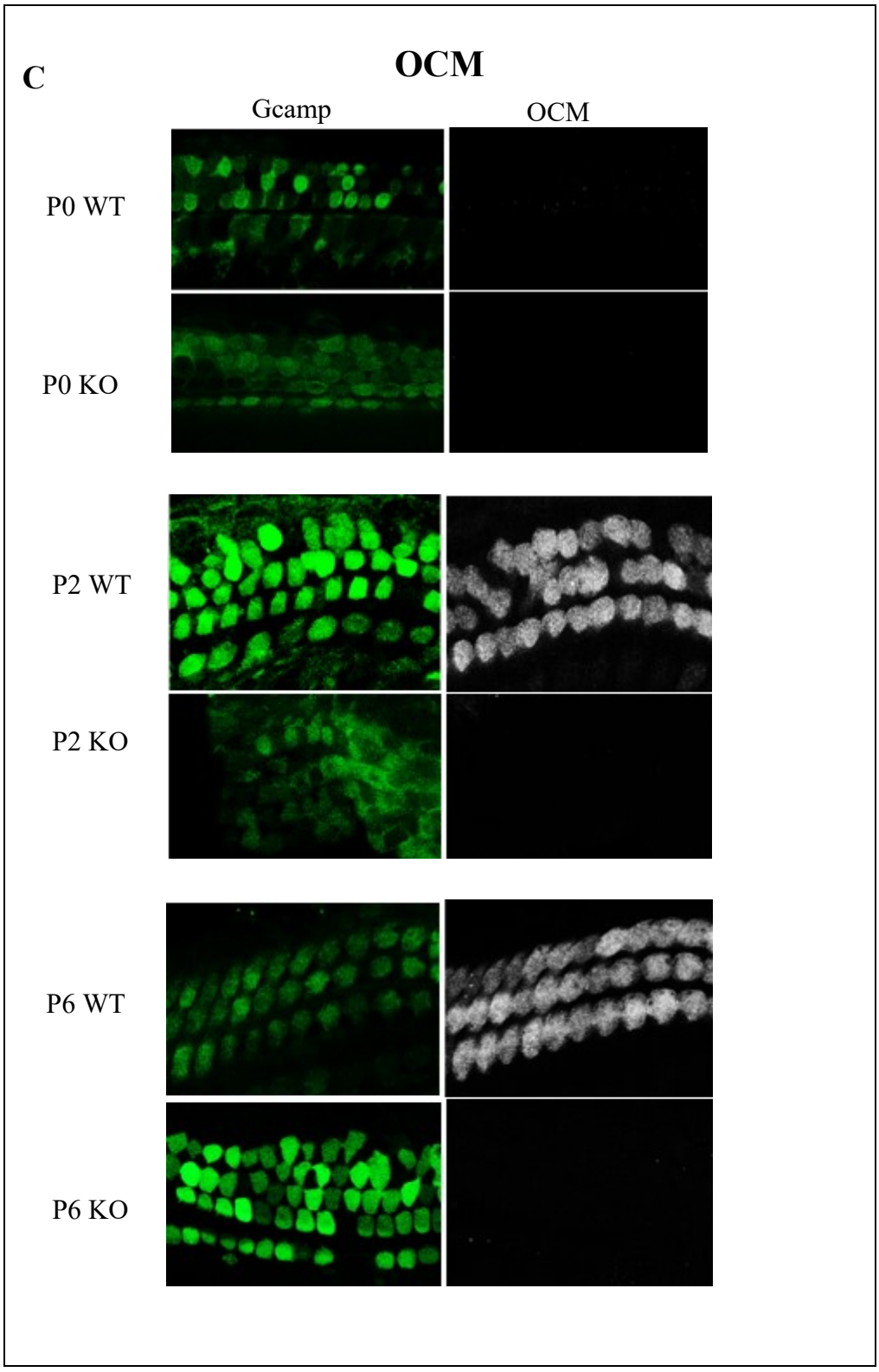
C
OCM
Gcamp
OCM
P0 WT
P0 KO
P2 WT
P2 KO
P6 WT
P6 KO

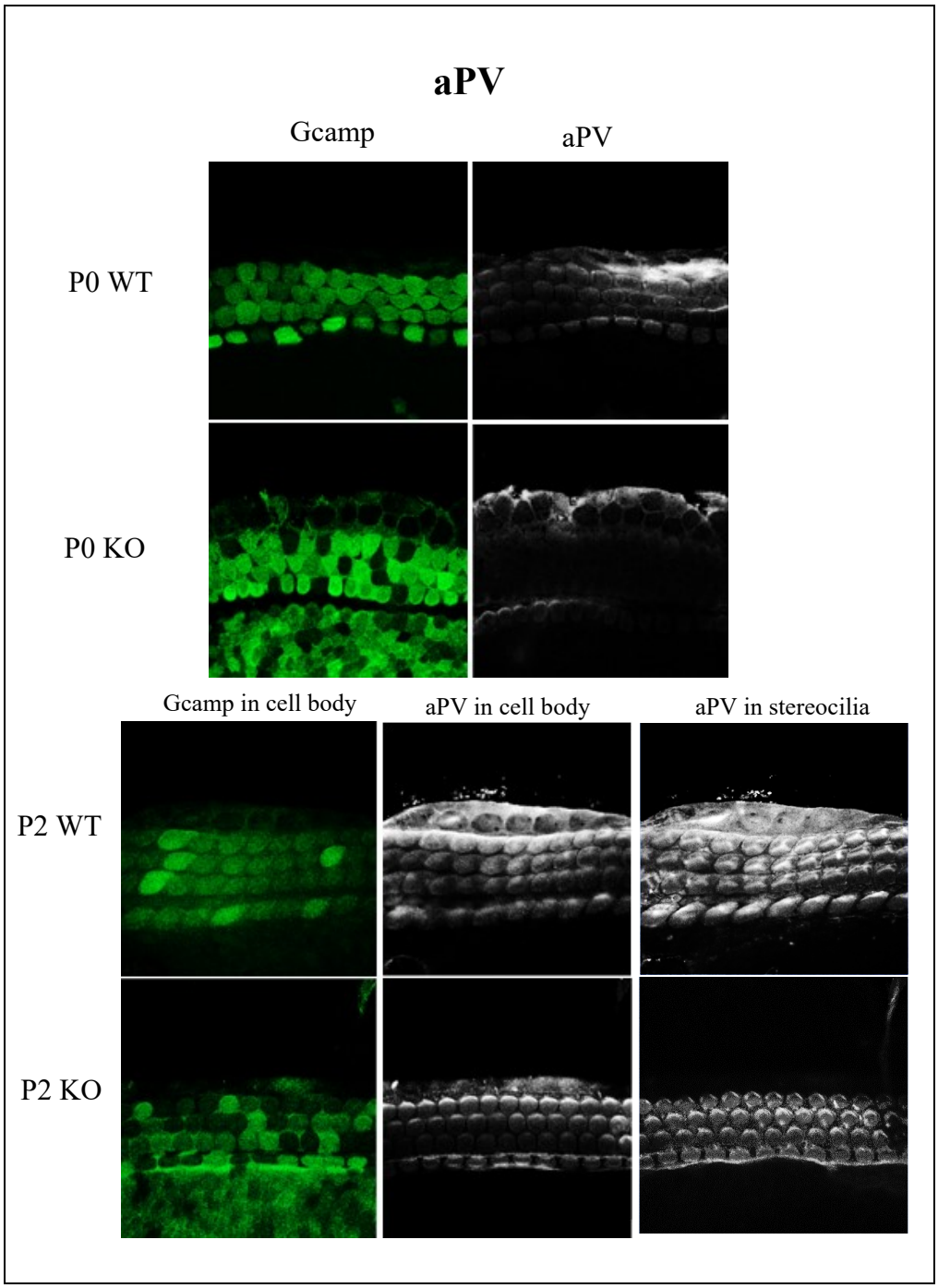
aPV
Gcamp
aPV
P0 WT
P0 KO
Gcamp in cell body
aPV in cell body
aPV in stereocilia
P2 WT
P2 KO

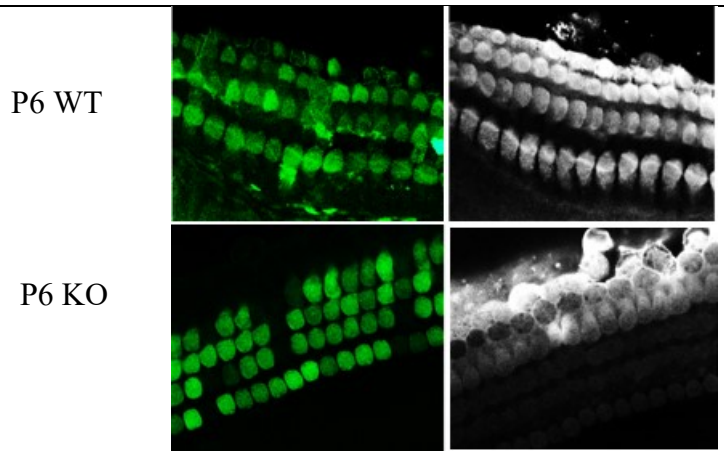

Figure 17. Relative gene expression for *Ocm*/OCM and *Pvalb*/aPV in Organ of Corti spirals from GCaMP6s+ mice at P0, P2, and P6. Plotted are the mean (± SD) mRNA levels normalized to P0 WT, which were determined using RT-qPCR. Asterisks (*) indicate a significant difference between WT and KO gene expression for the same age ($p < 0.05$, unpaired t-test). A-B) 2 different graphical representations of the same data that enable the viewer to see relative expression (A) and longitudinal expression more easily (B). $n = 2$-4 for each group. C) Immunohistochemistry images taken at 63x. Two aPV P2 images have been included for bot WT and KO in order to show their expression at the subcuticular and supracuticular regions of the OHCs. Specifically, the supracuticular region OHCs show aPV localization to the stereocilia, especially in KO mice. Green channel represents GCaMP, a HC marker.

CHAPTER FOUR

Discussion

In the absence of OCM, several important OHC Ca^{2+} regulators experienced altered gene and/or protein expression. This finding could suggest that OCM plays a role in the regulation or maintenance of Ca^{2+} signaling pathways in OHCs. This project examined how gene and/or protein expression for VGCCs (*Cacna1c*/$Ca_v1.2$, *Cacna1d*/$Ca_v1.3$), ionotropic purinergic receptors (*P2rx2*/P2X2, *P2rx3*/P2X3, *P2rx7*/P2X7), a Ca^{2+} extruder (*Atp2b2*/PMCA2), and a mobile Ca^{2+} buffer (*Pvalb*/aPV) developed differently without OCM. The data illuminated potential roles of OCM within OHCs, which will now be discussed.

4.1 Effects of OCM on OHC Ca^{2+} importers

Cacna1c and *Cacna1d* had a general reduction in mRNA expression in *Ocm* KO mice in comparison to WT mice at P0. This is fascinating because OCM does not begin protein expression until P2 in mice, yet its genetic removal downregulates the expression of important VGCCs in the OHC membrane. One hypothesis is that *Ocm* is involved with pathways regulating the expression of Ca^{2+} regulators. Such pathways are likely involved with the development and maintenance of hearing and could be the agent behind the change in VGCC mRNA expression prior to P2. How exactly this would occur is unknown.

From P0-P6, *Cacna1c* and *Cacna1d* were downregulated in the absence of OCM. Downregulating VGCC gene expression could be a response to decreased levels of Ca^{2+} buffer and sensor in the OHC. Decreasing the density of Ca^{2+} importers would reduce the damaging effects of having too much intracellular Ca^{2+} in the absence of enough intracellular Ca^{2+} buffer (e.g., OCM).

Cacna1c and *Cacna1d* also experienced a decrease in mRNA expression with age in both WT and KO mice. This is consistent with the findings of Qi et al. (2019) which showed that VGCC expression in HCs decrease with age. One explanation for the concurrent rise of *Ocm* and fall of *Cacna1c* and *Cacna1d* mRNA in WT mice is that other Ca^{2+} importers such as nAChRs and purinergic receptors begin to contribute to OHC Ca^{2+} influx, thereby reducing the need for VGCCs in such high quantities. Indeed, our data shows that *P2rx2* mRNA expression rises with the fall of *Cacna1c* and *Cacna1d* mRNA (P2-P6).

In contrast to VGCCs, purinergic receptors exhibited greater mRNA expression in *Ocm* KO mice than in *Ocm* WT mice. *P2rx2*, the most highly expressed of the OHC purinergic receptors considered, had a significant reduction in mRNA expression after P2 as if the missing "rise of OCM" did not sustain *P2rx2* expression in OHCs. In KO mice, most of the upregulated *P2rx2, P2rx3*, and *P2rx7* mRNA expression occurred before or at OCM onset. In WT mice, *P2rx2* mRNA expression rose while P2X3 and P2X7 mRNA expression was stagnant or decreased with age. This is consistent with the findings of Nikolic et al. (2003) in rats. In contrast to Brändle et al. (1999) and (Nikolic et al. (2003), however, this project and Scheffer et al. (2015) detected the presence of P2X3 in the

OHC. With the exception of *Cacna1d*, the mRNA expression levels collected for OHC VGCCs and purinergic receptors are similar to single cell (OHC) RNA Seq data from Scheffer et al. (2015; Fig. 18). Also, the fact that *P2rx2* and *P2rx3* expression patterns differed suggests that heteromeric P2X2/3 is probably not prevalent in OHCs.

Immunohistochemistry findings largely resemble the RT-qPCR data. An interesting exception, however, was P2X7. P2X7 demonstrated strong immunolabeling in stereocilia in P6 KO mice. It is not known why P2X7 would localize to stereocilia in maturing OHCs without OCM.

Considering the changes in expression levels for Ca^{2+} exporters in *Ocm* KO mice, OCM may increase VGCC expression and decrease *P2rx2* expression in OHCs.

4.2 Effect of OCM on an OHC Ca^{2+} exporter

Atp2b2 mRNA expression patterns were different between *Ocm* WT and *Ocm* KO mice. As was the case for OHC VGCCs and purinergic receptors, *Atp2b2* in KO mice had elevated mRNA expression at P0. Again, this could be the result of OCM's role in a regulatory network for OHC Ca^{2+} regulator proteins. At P2, *Atp2b2* mRNA expression in KO mice dropped below expression in WT mice. A drop in PMCA2 mRNA expression at P2 suggests that OCM plays a role in maintenance of *Atp2b2* expression. By P6, *Atp2b2* mRNA expression in KO mice surpasses expression in WT mice. Greater *Atp2b2* mRNA expression in the absence of OCM suggests that *Atp2b2* may undergo compensatory upregulation to meet the demands of an OHC without an essential Ca^{2+} buffer. In other words, more PMCA2 is needed to extrude the greater amounts of intracellular Ca^{2+}. Ca^{2+}

overload in the OHC can cause formation of reactive oxygen species, resulting in OHC death and deterioration of hearing. This is a phenomenon that can occur without adequate PMCA2 function (Fettiplace and Nam, 2019). Thus, upregulation of *Atp2b2* mRNA in the absence of OCM may promote OHC survival. This is likely unsustainable, though, as absence of OCM causes OHC damage and deafness as early as 4 months (Tong et al., 2016).

4.3 Effect of OCM on aPV

While OCM and aPV are similar in structure, function, and location, they are even more intertwined that previously expected. Counterintuitively, our data suggests that aPV is downregulated in the absence of OCM. Simultaneous downregulation of *Ocm*/OCM and *Pvalb*/aPV in OCM KO mice is counterintuitive because without OCM, aPV should take a bigger role in the maintenance of intracellular Ca^{2+}. However, compensatory increase in aPV expression was not observed in either RT-qPCR or immunohistochemistry experiments. Interestingly, Simmons et al. (2010) have shown that during development, OCM and aPV have inverse trends of expression, with OCM rising and aPV falling. This could be interpreted as aPV "handing" OCM the torch of OHC Ca^{2+} regulation. Nonetheless, the direct correlation between OCM and aPV expression in KO mice suggests that OCM plays a role in maintaining *Pvalb*/aPV expression in OHCs, at least during development.

The fact that *Pvalb* mRNA expression is significantly reduced at all ages in KO mice suggests that OCM plays a role in the activation, maintenance, or functionality of aPV in

the OHC. Additionally, the fact that *Pvalb* mRNA decreases from P2-P6 in WT mice suggests that OCM is involved with aPV downregulation. *Pvalb*/aPV downregulation could point to OCM's role in a feedback loop inhibiting the overexpression of intracellular [Ca^{2+} buffer]. While this is conjecture, there is currently no research that explains the relationship between OCM and aPV expression.

Immunohistochemistry data was relatively consistent with RT-qPCR findings. aPV had lower expression in KO mice than in WT mice. Where there seemed to be high expression levels of aPV in KO mice, expression was normally localized to stereocilia and not the OHC body. This suggests that aPV could move into the stereocilia in maturing KO mice, possibly to help buffer the increased levels of Ca^{2+} entering that region of the cell from the increased presence of P2X7 in stereocilia.

For *Cacna1d*/$Ca_v1.3$, *Atp2b2*/PMCA2, and *Pvalb*/aPV, our RT-qPCR/immunohistochemistry data were different from the single cell RNA Seq data seen in Fig. 18.

Figure 18. Absolute mRNA expression levels in OHCs isolated by fluorescence-activated cell sorting (FACS). RNA seq data taken from Scheffer et al. (2015). E16 = embryonic day 16; Cp = Cre+ (or OHC). With the exception of *Cacna1d, Atp2b2,* and *Pvalb*, our mRNA expression levels are similar to those found in this paper. It is unclear why there are discrepancies between $Ca_v1.3$ and aPV mRNA expression.

4.4 Summary and future directions

In OHCs, the absence of OCM causes a general downregulation in VGCCs, a general upregulation in purinergic receptors, a compensatory expression in PMCA2, and a downregulation of aPV. Broadly, the data shows that the regulation of OHC Ca^{2+} is multifactorial, meaning that many proteins are intricately involved with Ca^{2+} regulation. This was evidenced by changes in Ca^{2+} regulator expression when OCM, an important OHC Ca^{2+} buffer, was removed from the OHC. While the OHC Ca2+-regulating network may alter expression to reestablish a Ca^{2+} balance within the OHC, the compensatory efforts are unsustainable, which is demonstrated by the progressive, early-onset hearing loss that occurs in the absence of OCM. Ultimately, the data from this project suggests that OCM plays a role in maintaining Ca^{2+} regulators' gene expression, even before the first expression of OCM at P2, in order to maintain Ca^{2+} balance within the OHC.

Practically, this data can be used to determine potential targets for gene therapy. 50% of inner ear disorders are caused by genetic mutations, so gene-altering therapies may be the future for preventing or treating hearing loss (Nist-Lund et al., 2019). Experiments in mice from Nist-Lund et al. suggest that gene therapy for hearing loss is already within reach. Specifically, they engineered synthetic adeno-associated viral vectors to insert the *Tmc1* gene in hearing deficient mice, which codes for the TMC1 protein. TMC1 plays an essential role in MET channel functionality in HC stereocilia. Their findings show that administering the viral *Tmc1* to hearing deficient mice improves HC survival and function. Considering the findings of our present study, artificially altering the expression of Ca^{2+} regulators in OHCs with adenoviruses could become a

method of treating hearing deficiencies. The goal is to reestablish Ca^{2+} balance in the OHC. Based on the results of this project, reestablishing Ca^{2+} balance would require gene therapy targeting *multiple* Ca^{2+} regulators. Multifactorial gene therapy experiments should be conducted in cell lines prior to animal testing.

Finally, this project has highlighted other areas of potential research. Further research must be conducted on *how* the presence or absence of *Ocm*/OCM alters the expression of OHC Ca^{2+} regulators. Other regulators of OHC Ca^{2+} signaling such as P2X1, P2X4, Sorcin, SK2, nAchRs, METs, and TMCs should be included in this analysis. Lastly, western blots and greater sample size for immunohistochemistry experiments should be used to confirm the findings of this project.

Abbreviation	*Meaning*
aPV	Alpha-parvalbumin
ACh	Acetylcholine
ATP	Adenosine triphosphate
B2M	Beta-2-microglobulin
BLAST	Basic local alignment search tool
Ca^{2+}	Calcium
CaBPs	Calcium-binding proteins
$Ca_v1.2/3$	Voltage-gated calcium channel 1.2/3
cDNA	Complementary deoxyribonucleic acid
CICR	Calcium-induced calcium release
Ct	Cycle threshold value
DAPI	4', 6-diamno-2-phenylindole
DCs	Deiter's cells
DNA	Deoxyribonucleic acid
DPOAE	Distortion product otoacoustic emissions
ER	Endoplasmic reticulum
GCaMP	Genetic cyclic adenosine monophosphate
gDNA	Genomic deoxyribonucleic acid
HC	Hair cells
IHCs	Inner hair cells
K^+	Potassium

KO	Knock out (mouse)
LoxP	Locus of X-over P1
mRNA	Messenger ribonucleic acid
MET	Mechanoelectric transducer channel
Mg^{2+}	Magnesium
nAChRs	Nicotinic acetylcholine receptors
NCBI	National center for biotechnology information
NHS-T	Natural horse serum-triton
OCM	Oncomodulin
OHC	Outer hair cell
P_	Postnatal day __
P2X2/3/7	ATP-gated P2X receptor cation channels 2,3 & 7
PMCA2	Plasma membrane calcium ATPase 2
RNA	Ribonucleic acid
ROS	Reactive oxygen species
RT-qPCR	Reverse transcription quantitative polymerase chain reaction
SANDD	Sinoatrial node dysfunction and deafness syndrome
SERCA	Sarcoplasmic/endoplasmic reticulum calcium ATPase
SK2	Small conductance potassium channel
TBP	TATA-binding protein

TM1/2	Transmembrane segment 1/2
TMC1	Transmembrane channel-like protein 1
VGCCs	Voltage-gated calcium channels
WHO	World Health Organization
WT	Wild-type (mouse)
Zn^{2+}	Zinc

BIBLIOGRAPHY

Baig, S. M., Koschak, A., Lieb, A., Gebhart, M., Dafinger, C., Nürnberg, G., Ali, A., Ahmad, I., Sinnegger-Brauns, M. J., Brandt, N., Engel, J., Mangoni, M. E., Farooq, M., Khan, H. U., Nürnberg, P., Striessnig, J., & Bolz, H. J. (2011). Loss of Cav1.3 (CACNA1D) function in a human channelopathy with bradycardia and congenital deafness. *Nature Neuroscience*, *14*(1), 77–84. https://doi.org/10.1038/nn.2694

Betlejewski, S. (2008a). Nauka a życie – historia markiza Alfonso Cortiego. *Otolaryngologia Polska*, *62*(3), 344–347. https://doi.org/10.1016/S0030-6657(08)70268-3

Betlejewski, S. (2008b). Nauka a życie – historia markiza Alfonso Cortiego. *Otolaryngologia Polska*, *62*(3), 344–347. https://doi.org/10.1016/S0030-6657(08)70268-3

Beurg, M., Fettiplace, R., Nam, J.-H., & Ricci, A. J. (2009). Localization of inner hair cell mechanotransducer channels using high-speed calcium imaging. *Nature Neuroscience*, *12*(5), 553–558. https://doi.org/10.1038/nn.2295

Brändle, U., Zenner, H.-P., & Ruppersberg, J. P. (1999). Gene expression of P2X-receptors in the developing inner ear of the rat. *Neuroscience Letters*, *273*(2), 105–108. https://doi.org/10.1016/S0304-3940(99)00648-5

Carafoli, E. (1991). Calcium pump of the plasma membrane. *Physiological Reviews*, *71*(1), 129–153. https://doi.org/10.1152/physrev.1991.71.1.129

Carafoli, Ernesto. (2011). The plasma membrane calcium pump in the hearing process: Physiology and pathology. *Science China. Life Sciences*, *54*(8), 686–690. https://doi.org/10.1007/s11427-011-4200-z

Carpinelli, M. R., Manning, M. G., Kile, B. T., & Rachel, A. B. (2013). Two ENU-Induced Alleles of Atp2b2 Cause Deafness in Mice. *PLoS ONE*, *8*(6), e67479. https://doi.org/10.1371/journal.pone.0067479

Chen, C., Skellett, R. A., Fallon, M., & Bobbin, R. P. (1998). Additional pharmacological evidence that endogenous ATP modulates cochlear mechanics. *Hearing Research*, *118*(1–2), 47–61. https://doi.org/10.1016/S0378-5955(98)00019-7

Climer, L. K., Cox, A. M., Reynolds, T. J., & Simmons, D. D. (2019). Oncomodulin: The Enigmatic Parvalbumin Protein. *Frontiers in Molecular Neuroscience*, *12*, 235. https://doi.org/10.3389/fnmol.2019.00235

Cockayne, D. A., Dunn, P. M., Zhong, Y., Rong, W., Hamilton, S. G., Knight, G. E., Ruan, H.-Z., Ma, B., Yip, P., Nunn, P., McMahon, S. B., Burnstock, G., & Ford, A. P. D. W. (2005). P2X $_2$ knockout mice and P2X $_2$ /P2X $_3$ double knockout mice reveal a role for the P2X $_2$ receptor subunit in mediating multiple sensory effects of ATP: Sensory deficits in P2X knockout mice. *The Journal of Physiology*, *567*(2), 621–639. https://doi.org/10.1113/jphysiol.2005.088435

Corns, L. F., Johnson, S. L., Roberts, T., Ranatunga, K. M., Hendry, A., Ceriani, F., Safieddine, S., Steel, K. P., Forge, A., Petit, C., Furness, D. N., Kros, C. J., & Marcotti, W. (2018). Mechanotransduction is required for establishing and maintaining mature inner hair cells and regulating efferent innervation. *Nature Communications*, *9*(1), 4015. https://doi.org/10.1038/s41467-018-06307-w

Cox, J. A., Milos, M., & MacManus, J. P. (1990). Calcium- and magnesium-binding properties of oncomodulin. Direct binding studies and microcalorimetry. *The Journal of Biological Chemistry*, *265*(12), 6633–6637.

Dallos, P., Popper, A. N., & Fay, R. R. (Eds.). (1996). *The Cochlea* (Vol. 8). Springer New York. https://doi.org/10.1007/978-1-4612-0757-3

Dechesne, C. J., Rabejac, D., & Desmadryl, G. (1994). Development of calretinin immunoreactivity in the mouse inner ear. *The Journal of Comparative Neurology*, *346*(4), 517–529. https://doi.org/10.1002/cne.903460405

Di Leva, F., Domi, T., Fedrizzi, L., Lim, D., & Carafoli, E. (2008). The plasma membrane Ca2+ ATPase of animal cells: Structure, function and regulation. *Archives of Biochemistry and Biophysics*, *476*(1), 65–74. https://doi.org/10.1016/j.abb.2008.02.026

Dong, Y., Zhang, C., Frye, M., Yang, W., Ding, D., Sharma, A., Guo, W., & Hu, B. H. (2018). Differential fates of tissue macrophages in the cochlea during postnatal development. *Hearing Research*, *365*, 110–126. https://doi.org/10.1016/j.heares.2018.05.010

Dou, H., Vazquez, AnaE., Namkung, Y., Chu, H., Cardell, E., Nie, L., Parson, S., Shin, H.-S., & Yamoah, EbenezerN. (2004). Null Mutation of ?1D Ca2+ Channel Gene Results in Deafness but No Vestibular Defect in Mice. *Journal of the Association for Research in Otolaryngology*, *5*(2). https://doi.org/10.1007/s10162-003-4020-3

Dumont, R. A., Lins, U., Filoteo, A. G., Penniston, J. T., Kachar, B., & Gillespie, P. G. (2001). Plasma Membrane Ca $^{2+}$ -ATPase Isoform 2a Is the PMCA of Hair Bundles. *The Journal of Neuroscience*, *21*(14), 5066–5078. https://doi.org/10.1523/JNEUROSCI.21-14-05066.2001

Fettiplace, R. (2016). Is TMC1 the Hair Cell Mechanotransducer Channel? *Biophysical Journal*, *111*(1), 3–9. https://doi.org/10.1016/j.bpj.2016.05.032

Fettiplace, R., & Nam, J.-H. (2019). Tonotopy in calcium homeostasis and vulnerability of cochlear hair cells. *Hearing Research*, *376*, 11–21. https://doi.org/10.1016/j.heares.2018.11.002

Ficarella, R., Di Leva, F., Bortolozzi, M., Ortolano, S., Donaudy, F., Petrillo, M., Melchionda, S., Lelli, A., Domi, T., Fedrizzi, L., Lim, D., Shull, G. E., Gasparini, P., Brini, M., Mammano, F., & Carafoli, E. (2007). A functional study of plasma-membrane calcium-pump isoform 2 mutants causing digenic deafness. *Proceedings of the National Academy of Sciences*, *104*(5), 1516–1521. https://doi.org/10.1073/pnas.0609775104

Fu, B., Le Prell, C., Simmons, D., Lei, D., Schrader, A., Chen, A. B., & Bao, J. (2010). Age-related synaptic loss of the medial olivocochlear efferent innervation. *Molecular Neurodegeneration*, *5*(1), 53. https://doi.org/10.1186/1750-1326-5-53

Furness, D. N. (2015). Molecular basis of hair cell loss. *Cell and Tissue Research*, *361*(1), 387–399. https://doi.org/10.1007/s00441-015-2113-z

Furuta, H., Luo, L., Hepler, K., & Ryan, A. F. (1998). Evidence for differential regulation of calcium by outer versus inner hair cells: Plasma membrane Ca-ATPase gene expression. *Hearing Research*, *123*(1–2), 10–26. https://doi.org/10.1016/S0378-5955(98)00091-4

George, B., Swartz, K. J., & Li, M. (2019). Hearing loss mutations alter the functional properties of human P2X2 receptor channels through distinct mechanisms. *Proceedings of the National Academy of Sciences*, *116*(45), 22862–22871. https://doi.org/10.1073/pnas.1912156116

Ghaffari, R., Aranyosi, A. J., & Freeman, D. M. (2007). Longitudinally propagating traveling waves of the mammalian tectorial membrane. *Proceedings of the National Academy of Sciences*, *104*(42), 16510–16515. https://doi.org/10.1073/pnas.0703665104

Goodman, M., & Pechére, J.-F. (1977). The evolution of muscular parvalbumins investigated by the maximum parsimony method. *Journal of Molecular Evolution*, *9*(2), 131–158. https://doi.org/10.1007/BF01732745

Hackney, C. M. (2005a). The Concentrations of Calcium Buffering Proteins in Mammalian Cochlear Hair Cells. *Journal of Neuroscience*, *25*(34), 7867–7875. https://doi.org/10.1523/JNEUROSCI.1196-05.2005

Hackney, C. M. (2005b). The Concentrations of Calcium Buffering Proteins in Mammalian Cochlear Hair Cells. *Journal of Neuroscience*, *25*(34), 7867–7875. https://doi.org/10.1523/JNEUROSCI.1196-05.2005

Hackney, Carole M., Mahendrasingam, S., Jones, E. M. C., & Fettiplace, R. (2003). The Distribution of Calcium Buffering Proteins in the Turtle Cochlea. *The Journal of*

Neuroscience, *23*(11), 4577–4589. https://doi.org/10.1523/JNEUROSCI.23-11-04577.2003

Hallworth, R. (1997). Modulation of outer hair cell compliance and force by agents that affect hearing. *Hearing Research*, *114*(1–2), 204–212. https://doi.org/10.1016/S0378-5955(97)00167-6

Hamard, P.-J., Lukin, D. J., & Manfredi, J. J. (2012). P53 Basic C Terminus Regulates p53 Functions through DNA Binding Modulation of Subset of Target Genes. *Journal of Biological Chemistry*, *287*(26), 22397–22407. https://doi.org/10.1074/jbc.M111.331298

Hapak, R. C., Lammers, P. J., Palmisano, W. A., Birnbaum, E. R., & Henzl, M. T. (1989). Site-specific substitution of glutamate for aspartate at position 59 of rat oncomodulin. *The Journal of Biological Chemistry*, *264*(31), 18751–18760.

Horakova, D., Zivadinov, R., Weinstock-Guttman, B., Havrdova, E., Qu, J., Tamaño-Blanco, M., Badgett, D., Tyblova, M., Bergsland, N., Hussein, S., Willis, L., Krasensky, J., Vaneckova, M., Seidl, Z., Lelkova, P., Dwyer, M. G., Zhang, M., Yu, H., Duan, X., … Ramanathan, M. (2013). Environmental Factors Associated with Disease Progression after the First Demyelinating Event: Results from the Multi-Center SET Study. *PLoS ONE*, *8*(1), e53996. https://doi.org/10.1371/journal.pone.0053996

Horáková, L., Strosova, M. K., Spickett, C. M., & Blaskovic, D. (2013). Impairment of calcium ATPases by high glucose and potential pharmacological protection. *Free Radical Research*, *47*(sup1), 81–92. https://doi.org/10.3109/10715762.2013.807923

Hu, R. L., Huang, G., Qiu, W., Zhong, Z. H., Xia, X. Z., & Yin, Z. (2001). [No title found]. *Veterinary Research Communications*, *25*(1), 77–84. https://doi.org/10.1023/A:1006417203856

Hu, Z., Liang, M., & Soong, T. (2017). Alternative Splicing of L-type CaV1.2 Calcium Channels: Implications in Cardiovascular Diseases. *Genes*, *8*(12), 344. https://doi.org/10.3390/genes8120344

Hudspeth, A. J. (2008). Making an Effort to Listen: Mechanical Amplification in the Ear. *Neuron*, *59*(4), 530–545. https://doi.org/10.1016/j.neuron.2008.07.012

Ilari, A., Fiorillo, A., Poser, E., Lalioti, V. S., Sundell, G. N., Ivarsson, Y., Genovese, I., & Colotti, G. (2015). Structural basis of Sorcin-mediated calcium-dependent signal transduction. *Scientific Reports*, *5*(1), 16828. https://doi.org/10.1038/srep16828

Illes, P., Müller, C. E., Jacobson, K. A., Grutter, T., Nicke, A., Fountain, S. J., Kennedy, C., Schmalzing, G., Jarvis, M. F., Stojilkovic, S. S., King, B. F., & Di Virgilio, F. (2021). Update of P2X receptor properties and their pharmacology: IUPHAR Review 30. *British Journal of Pharmacology*, *178*(3), 489–514. https://doi.org/10.1111/bph.15299

J. Lim, D. (1987). Development of the tectorial membrane. *Hearing Research*, *28*(1), 9–21. https://doi.org/10.1016/0378-5955(87)90149-3

Jeng, J., Ceriani, F., Hendry, A., Johnson, S. L., Yen, P., Simmons, D. D., Kros, C. J., & Marcotti, W. (2019). Hair cell maturation is differentially regulated along the tonotopic axis of the mammalian cochlea. *The Journal of Physiology*, JP279012. https://doi.org/10.1113/JP279012

Jeng, J., Ceriani, F., Olt, J., Brown, S. D. M., Holley, M. C., Bowl, M. R., Johnson, S. L., & Marcotti, W. (2020). Pathophysiological changes in inner hair cell ribbon synapses in the ageing mammalian cochlea. *The Journal of Physiology*, *598*(19), 4339–4355. https://doi.org/10.1113/JP280018

Jiang, L.-H., Kim, M., Spelta, V., Bo, X., Surprenant, A., & North, R. A. (2003). Subunit Arrangement in P2X Receptors. *The Journal of Neuroscience*, *23*(26), 8903–8910. https://doi.org/10.1523/JNEUROSCI.23-26-08903.2003

Johnson, S. L., Beurg, M., Marcotti, W., & Fettiplace, R. (2011). Prestin-Driven Cochlear Amplification Is Not Limited by the Outer Hair Cell Membrane Time Constant. *Neuron*, *70*(6), 1143–1154. https://doi.org/10.1016/j.neuron.2011.04.024

Khakh, B. S., & Alan North, R. (2006). P2X receptors as cell-surface ATP sensors in health and disease. *Nature*, *442*(7102), 527–532. https://doi.org/10.1038/nature04886

Khimich, D., Nouvian, R., Pujol, R., tom Dieck, S., Egner, A., Gundelfinger, E. D., & Moser, T. (2005). Hair cell synaptic ribbons are essential for synchronous auditory signalling. *Nature*, *434*(7035), 889–894. https://doi.org/10.1038/nature03418

Kimura, T., Tajiri, K., Sato, A., Sakai, S., Wang, Z., Yoshida, T., Uede, T., Hiroe, M., Aonuma, K., Ieda, M., & Imanaka-Yoshida, K. (2019). Tenascin-C accelerates adverse ventricular remodelling after myocardial infarction by modulating macrophage polarization. *Cardiovascular Research*, *115*(3), 614–624. https://doi.org/10.1093/cvr/cvy244

Knipper, M., Zimmermann, U., Rohbock, K., Köpschall, I., & Zenner, H. P. (1995). Synaptophysin and GAP-43 proteins in efferent fibers of the inner ear during postnatal development. *Brain Research. Developmental Brain Research*, *89*(1), 73–86. https://doi.org/10.1016/0165-3806(95)00113-r

Kozel, P. J., Davis, R. R., Krieg, E. F., Shull, G. E., & Erway, L. C. (2002). Deficiency in plasma membrane calcium ATPase isoform 2 increases susceptibility to noise-induced hearing loss in mice. *Hearing Research*, *164*(1–2), 231–239. https://doi.org/10.1016/S0378-5955(01)00420-8

Kubo, Y., Fujiwara, Y., Keceli, B., & Nakajo, K. (2009). Dynamic aspects of functional regulation of the ATP receptor channel P2X $_2$: Regulation of the ATP receptor channel P2X $_2$. *The Journal of Physiology*, *587*(22), 5317–5324. https://doi.org/10.1113/jphysiol.2009.179309

Kushnir, A., & Marx, S. O. (2018). Voltage-Gated Calcium Channels. In *Cardiac Electrophysiology: From Cell to Bedside* (pp. 12–24). Elsevier. https://doi.org/10.1016/B978-0-323-44733-1.00002-X

Kwiatkowska, M., Reinhard, J., Roll, L., Kraft, N., Dazert, S., Faissner, A., & Volkenstein, S. (2016). The expression pattern and inhibitory influence of Tenascin-C on the growth of spiral ganglion neurons suggest a regulatory role as boundary formation molecule in the postnatal mouse inner ear. *Neuroscience*, *319*, 46–58. https://doi.org/10.1016/j.neuroscience.2016.01.039

Letourneau, P. (2009). Axonal Pathfinding: Extracellular Matrix Role. In *Encyclopedia of Neuroscience* (pp. 1139–1145). Elsevier. https://doi.org/10.1016/B978-008045046-9.00335-1

Lewin, G. R., & Moshourab, R. (2004). Mechanosensation and pain. *Journal of Neurobiology*, *61*(1), 30–44. https://doi.org/10.1002/neu.20078

Liberman, L., & Liberman, M. (2019). Cochlear efferent innervation is sparse in humans and decreases with age. *The Journal of Neuroscience*, 3004–3018. https://doi.org/10.1523/JNEUROSCI.3004-18.2019

Liberman, M. C., Gao, J., He, D. Z. Z., Wu, X., Jia, S., & Zuo, J. (2002). Prestin is required for electromotility of the outer hair cell and for the cochlear amplifier. *Nature*, *419*(6904), 300–304. https://doi.org/10.1038/nature01059

Lipscombe, D., Helton, T. D., & Xu, W. (2004). L-Type Calcium Channels: The Low Down. *Journal of Neurophysiology*, *92*(5), 2633–2641. https://doi.org/10.1152/jn.00486.2004

Liu, X. Z. (2003). Prestin, a cochlear motor protein, is defective in non-syndromic hearing loss. *Human Molecular Genetics*, *12*(10), 1155–1162. https://doi.org/10.1093/hmg/ddg127

Livak, K. J., & Schmittgen, T. D. (2001). Analysis of Relative Gene Expression Data Using Real-Time Quantitative PCR and the 2−ΔΔCT Method. *Methods*, *25*(4), 402–408. https://doi.org/10.1006/meth.2001.1262

Localization of cholinergic and purinergic receptors on outer hair cells isolated from the guinea-pig cochlea. (1992). *Proceedings of the Royal Society of London. Series B: Biological Sciences*, *249*(1326), 265–273. https://doi.org/10.1098/rspb.1992.0113

Maroonroge, S., Emanuel, D., & Letowski, T. (2009). *Basic anatomy of the hearing system* (pp. 279–306).

McCullough, B. J., & L. Tempel, B. (2004). Haplo-insufficiency revealed in deafwaddler mice when tested for hearing loss and ataxia. *Hearing Research*, *195*(1–2), 90–102. https://doi.org/10.1016/j.heares.2004.05.003

Meskell, M. (2010). Principles of Anatomy and Physiology. *Journal of Anatomy*, *217*(5), 631–631. https://doi.org/10.1111/j.1469-7580.2010.01292.x

Moncrief, N. D., Kretsinger, R. H., & Goodman, M. (1990). Evolution of EF-hand calcium-modulated proteins. I. Relationships based on amino acid sequences. *Journal of Molecular Evolution*, *30*(6), 522–562. https://doi.org/10.1007/BF02101108

Morley, B. J., Dolan, D. F., Ohlemiller, K. K., & Simmons, D. D. (2017). Generation and Characterization of α9 and α10 Nicotinic Acetylcholine Receptor Subunit Knockout Mice on a C57BL/6J Background. *Frontiers in Neuroscience*, *11*, 516. https://doi.org/10.3389/fnins.2017.00516

Nagaya, N., Tittle, R. K., Saar, N., Dellal, S. S., & Hume, R. I. (2005). An Intersubunit Zinc Binding Site in Rat P2X2 Receptors. *Journal of Biological Chemistry*, *280*(28), 25982–25993. https://doi.org/10.1074/jbc.M504545200

Nist-Lund, C. A., Pan, B., Patterson, A., Asai, Y., Chen, T., Zhou, W., Zhu, H., Romero, S., Resnik, J., Polley, D. B., Géléoc, G. S., & Holt, J. R. (2019). Improved TMC1 gene therapy restores hearing and balance in mice with genetic inner ear disorders. *Nature Communications*, *10*(1), 236. https://doi.org/10.1038/s41467-018-08264-w

North, R. A. (2002). Molecular Physiology of P2X Receptors. *Physiological Reviews*, *82*(4), 1013–1067. https://doi.org/10.1152/physrev.00015.2002

Nouvian, R., Neef, J., Bulankina, A. V., Reisinger, E., Pangršič, T., Frank, T., Sikorra, S., Brose, N., Binz, T., & Moser, T. (2011). Exocytosis at the hair cell ribbon synapse apparently operates without neuronal SNARE proteins. *Nature Neuroscience*, *14*(4), 411–413. https://doi.org/10.1038/nn.2774

Observations on the electrochemistry of the cochlear endolymph of the rat: A quantitative study of its electrical potential and ionic composition as determined by means of flame spectrophotometry. (1968). *Proceedings of the Royal Society of London. Series B. Biological Sciences*, *171*(1023), 227–247. https://doi.org/10.1098/rspb.1968.0066

Pak, A. K., & Slepecky, N. B. (1995). Cytoskeletal and calcium-binding proteins in the mammalian organ of Corti: Cell type-specific proteins displaying longitudinal and radial gradients. *Hearing Research*, *91*(1–2), 119–135. https://doi.org/10.1016/0378-5955(95)00173-5

Patuzzi, R. B., Yates, G. K., & Johnstone, B. M. (1989). Outer hair cell receptor current and sensorineural hearing loss. *Hearing Research*, *42*(1), 47–72. https://doi.org/10.1016/0378-5955(89)90117-2

Pauls, T. L., Cox, J. A., & Berchtold, M. W. (1996). The Ca2+-binding proteins parvalbumin and oncomodulin and their genes: New structural and functional findings. *Biochimica et Biophysica Acta (BBA) - Gene Structure and Expression*, *1306*(1), 39–54. https://doi.org/10.1016/0167-4781(95)00221-9

Permyakov, S. E., Bakunts, A. G., Denesyuk, A. I., Knyazeva, E. L., Uversky, V. N., & Permyakov, E. A. (2008). Apo-parvalbumin as an intrinsically disordered protein. *Proteins: Structure, Function, and Bioinformatics*, *72*(3), 822–836. https://doi.org/10.1002/prot.21974

Pickles, James O. (1988). *An introduction to the physiology of hearing* (2nd ed). Academic Press.

Pickles, J.O., Comis, S. D., & Osborne, M. P. (1984). Cross-links between stereocilia in the guinea pig organ of Corti, and their possible relation to sensory transduction. *Hearing Research*, *15*(2), 103–112. https://doi.org/10.1016/0378-5955(84)90041-8

Prades, S., Heard, G., Gale, J. E., Engel, T., Kopp, R., Nicke, A., Smith, K. E., & Jagger, D. J. (2021). Functional P2X $_7$ receptors in the auditory nerve of hearing rodents localize exclusively to peripheral glia. *The Journal of Neuroscience*, JN-RM-2240-20. https://doi.org/10.1523/JNEUROSCI.2240-20.2021

Qi, F., Zhang, R., Chen, J., Zhao, F., Sun, Y., Du, Z., Bing, D., Li, P., Shao, S., Zhu, H., & Chu, H. (2019). Down-regulation of Cav1.3 in auditory pathway promotes age-related hearing loss by enhancing calcium-mediated oxidative stress in male mice. *Aging*, *11*(16), 6490–6502. https://doi.org/10.18632/aging.102203

Ranum, P. T., Goodwin, A. T., Yoshimura, H., Kolbe, D. L., Walls, W. D., Koh, J.-Y., He, D. Z. Z., & Smith, R. J. H. (2019). Insights into the Biology of Hearing and Deafness Revealed by Single-Cell RNA Sequencing. *Cell Reports*, *26*(11), 3160-3171.e3. https://doi.org/10.1016/j.celrep.2019.02.053

Roberts, J. A., Vial, C., Digby, H. R., Agboh, K. C., Wen, H., Atterbury-Thomas, A., & Evans, R. J. (2006). Molecular properties of P2X receptors. *Pflügers Archiv - European Journal of Physiology*, *452*(5), 486–500. https://doi.org/10.1007/s00424-006-0073-6

Scheffer, D. I., Shen, J., Corey, D. P., & Chen, Z.-Y. (2015). Gene Expression by Mouse Inner Ear Hair Cells during Development. *Journal of Neuroscience*, *35*(16), 6366–6380. https://doi.org/10.1523/JNEUROSCI.5126-14.2015

Schwaller, B. (2009). The continuing disappearance of "pure" Ca2+ buffers. *Cellular and Molecular Life Sciences*, *66*(2), 275–300. https://doi.org/10.1007/s00018-008-8564-6

Schwaller, B. (2010). Cytosolic Ca2+ Buffers. *Cold Spring Harbor Perspectives in Biology*, *2*(11), a004051–a004051. https://doi.org/10.1101/cshperspect.a004051

Schwaller, Beat. (2014). Calretinin: From a "simple" Ca2+ buffer to a multifunctional protein implicated in many biological processes. *Frontiers in Neuroanatomy*, *8*. https://doi.org/10.3389/fnana.2014.00003

Schwaller, Beat, Meyer, M., & Schiffmann, S. (2002). "New" functions for "old" proteins: The role of the calcium-binding proteins calbindin D-28k, calretinin and parvalbumin, in cerebellar physiology. Studies with knockout mice. *The Cerebellum*, *1*(4), 241–258. https://doi.org/10.1080/147342202320883551

Siegel, G. J. (2006). *Basic neurochemistry: Molecular, cellular and medical aspects*. http://site.ebrary.com/id/10169920

Simmons, D. D. (2002). Developmental mRNA expression of the α10 nicotinic acetylcholine receptor subunit in the rat cochlea. *Developmental Brain Research*, *139*(1), 87–96. https://doi.org/10.1016/S0165-3806(02)00514-X

Simmons, D. D., Tong, B., Schrader, A. D., & Hornak, A. J. (2010). Oncomodulin identifies different hair cell types in the mammalian inner ear. *The Journal of Comparative Neurology*, *518*(18), 3785–3802. https://doi.org/10.1002/cne.22424

Sobkowicz, H. M., Inagaki, M., August, B. K., & Slapnick, S. M. (1999). [No title found]. *Journal of Neurocytology*, *28*(1), 17–38. https://doi.org/10.1023/A:1007059616607

Sonntag, M., Blosa, M., Schmidt, S., Reimann, K., Blum, K., Eckrich, T., Seeger, G., Hecker, D., Schick, B., Arendt, T., Engel, J., & Morawski, M. (2018). Synaptic coupling of inner ear sensory cells is controlled by brevican-based extracellular matrix baskets resembling perineuronal nets. *BMC Biology*, *16*(1), 99. https://doi.org/10.1186/s12915-018-0566-8

Soto-Prior, A., Cluzel, M., Renard, N., Ripoll, C., Lavigne-Rebillard, M., Eybalin, M., & Hamel, C. P. (1995). Molecular cloning and expression of α parvalbumin in the guinea pig cochlea. *Molecular Brain Research*, *34*(2), 337–342. https://doi.org/10.1016/0169-328X(95)00205-7

Spandidos, A., Wang, X., Wang, H., Dragnev, S., Thurber, T., & Seed, B. (2008). A comprehensive collection of experimentally validated primers for Polymerase Chain Reaction quantitation of murine transcript abundance. *BMC Genomics*, *9*(1), 633. https://doi.org/10.1186/1471-2164-9-633

Spandidos, A., Wang, X., Wang, H., & Seed, B. (2010). PrimerBank: A resource of human and mouse PCR primer pairs for gene expression detection and quantification. *Nucleic Acids Research*, *38*(suppl_1), D792–D799. https://doi.org/10.1093/nar/gkp1005

Spinelli, K. J., & Gillespie, P. G. (2009). Bottoms up: Transduction channels at tip link bases. *Nature Neuroscience*, *12*(5), 529–530. https://doi.org/10.1038/nn0509-529

Szücs, A., Szappanos, H., Tóth, A., Farkas, Z., Panyi, G., Csernoch, L., & Sziklai, I. (2004). Differential expression of purinergic receptor subtypes in the outer hair cells of the guinea pig. *Hearing Research*, *196*(1–2), 2–7. https://doi.org/10.1016/j.heares.2004.04.008

Tan, X., Beurg, M., Hackney, C., Mahendrasingam, S., & Fettiplace, R. (2013). Electrical tuning and transduction in short hair cells of the chicken auditory papilla. *Journal of Neurophysiology*, *109*(8), 2007–2020. https://doi.org/10.1152/jn.01028.2012

Tateya, T., Sakamoto, S., Ishidate, F., Hirashima, T., Imayoshi, I., & Kageyama, R. (2019). Three-dimensional live imaging of Atoh1 reveals the dynamics of hair cell induction and organization in the developing cochlea. *Development*, *146*(21), dev177881. https://doi.org/10.1242/dev.177881

Thalmann, I., Thallinger, G., Comegys, T. H., & Thalmann, R. (1986). Collagen – The Predominant Protein of the Tectorial Membrane. *ORL*, *48*(2), 107–115. https://doi.org/10.1159/000275855

Tong, B., Hornak, A. J., Maison, S. F., Ohlemiller, K. K., Liberman, M. C., & Simmons, D. D. (2016). Oncomodulin, an EF-Hand Ca $^{2+}$ Buffer, Is Critical for Maintaining Cochlear Function in Mice. *The Journal of Neuroscience*, *36*(5), 1631–1635. https://doi.org/10.1523/JNEUROSCI.3311-15.2016

Vikhe Patil, K., Canlon, B., & Cederroth, C. R. (2015). High quality RNA extraction of the mammalian cochlea for qRT-PCR and transcriptome analyses. *Hearing Research*, *325*, 42–48. https://doi.org/10.1016/j.heares.2015.03.008

Vyas, P., Wu, J. S., Zimmerman, A., Fuchs, P., & Glowatzki, E. (2017). Tyrosine Hydroxylase Expression in Type II Cochlear Afferents in Mice. *Journal of the Association for Research in Otolaryngology*, *18*(1), 139–151. https://doi.org/10.1007/s10162-016-0591-7

Wang, X., Spandidos, A., Wang, H., & Seed, B. (2012). PrimerBank: A PCR primer database for quantitative gene expression analysis, 2012 update. *Nucleic Acids Research*, *40*(D1), D1144–D1149. https://doi.org/10.1093/nar/gkr1013

Whitlon, D. S., Zhang, X., & Kusakabe, M. (1999). Tenascin-C in the cochlea of the developing mouse. *The Journal of Comparative Neurology*, *406*(3), 361–374. https://doi.org/10.1002/(sici)1096-9861(19990412)406:3<361::aid-cne5>3.0.co;2-o

Wu, J. S., Vyas, P., Glowatzki, E., & Fuchs, P. A. (2018). Opposing expression gradients of calcitonin-related polypeptide alpha (*Calca* / *Cgrp* α) and tyrosine hydroxylase (*Th*) in type II afferent neurons of the mouse cochlea. *Journal of Comparative Neurology*, *526*(3), 425–438. https://doi.org/10.1002/cne.24341

Yamoah, E. N., Li, M., Shah, A., Elliott, K. L., Cheah, K., Xu, P.-X., Phillips, S., Young, S. M., Eberl, D. F., & Fritzsch, B. (2020). Using Sox2 to alleviate the hallmarks of age-related hearing loss. *Ageing Research Reviews*, *59*, 101042. https://doi.org/10.1016/j.arr.2020.101042

Yan, D., Zhu, Y., Walsh, T., Xie, D., Yuan, H., Sirmaci, A., Fujikawa, T., Wong, A. C. Y., Loh, T. L., Du, L., Grati, M., Vlajkovic, S. M., Blanton, S., Ryan, A. F., Chen, Z.-Y., Thorne, P. R., Kachar, B., Tekin, M., Zhao, H.-B., … Liu, X. Z. (2013). Mutation of the ATP-gated P2X2 receptor leads to progressive hearing loss and increased susceptibility to noise. *Proceedings of the National Academy of Sciences*, *110*(6), 2228–2233. https://doi.org/10.1073/pnas.1222285110

Yang, D., Thalmann, I., Thalmann, R., & Simmons, D. D. (2004). Expression of ? And ? parvalbumin is differentially regulated in the rat organ of corti during development. *Journal of Neurobiology*, *58*(4), 479–492. https://doi.org/10.1002/neu.10289